Tumor-derived interleukin-34 creates an immunosuppressive and chemoresistant tumor microenvironment by modulating myeloid-derived suppressor cells in triple-negative breast cancer

Nabeel Kajihara[1], Takuto Kobayashi[1], Ryo Otsuka[1], Junko Nio-Kobayashi[2], Tomohiro Oshino[3], Masato Takahashi[3], Seiichi Imanishi[4], Ari Hashimoto[5], Haruka Wada[1], Ken-ichiro Seino[1]

AUTHOR AFFILIATIONS

[1]Division of Immunobiology, Graduate School of Medicine, Institute for Genetic Medicine, Hokkaido University, Kita-15 Nishi-7, Kita-ku, Sapporo city, Hokkaido 060-0815, Japan

[2]Laboratory of Histology and Cytology, Graduate School of Medicine, Hokkaido University, Kita-15 Nishi-7, Kita-ku, Sapporo city, Hokkaido 060-8638, Japan

[3]Department of Breast Surgery, Hokkaido University Hospital, Kita-14 Nishi-5, Kita-ku, Sapporo city, Hokkaido 060-8648, Japan

[4]Department of Breast Surgery, Osaka Rosai Hospital, Nagasone-cho 1179-3, Kita-ku, Sakai city, Osaka 591-8025, Japan

[5]Department of Molecular Biology, Faculty of Medicine, Hokkaido University, Kita-15 Nishi-7, Kita-ku, Sapporo city, Hokkaido 060-8638, Japan

CORRESPONDING AUTHOR

Ken-ichiro Seino, M.D., Ph.D.

Division of Immunobiology, Graduate School of Medicine, Institute for Genetic Medicine, Hokkaido University, Kita-15 Nishi-7, Kita-ku, Sapporo city, Hokkaido 060-0815, Japan

Tel: 81-11-706-5532, Fax: 81-11-706-7545, E-mail: seino@igm.hokudai.ac.jp

ABSTRACT

Triple-negative breast cancer (TNBC) is an aggressive breast cancer subtype characterized by a lack of therapeutic targets. The paucity of effective treatment options motivated a number of studies to tackle this problem. Immunosuppressive cells infiltrated into the tumor microenvironment (TME) of TNBC are currently considered as candidates for new therapeutic targets. Myeloid-derived suppressor cells (MDSCs) have been reported to populate in the TME of TNBC, but their roles in the clinical and biological features of TNBC have not been clarified. This study identified that interleukin-34 (IL-34) released by TNBC cells is a crucial immunomodulator to regulate MDSCs accumulation in the TME. We provide evidence that IL-34 induces a differentiation of myeloid stem cells into monocytic MDSCs (M-MDSCs) that recruits regulatory T (Treg) cells, while suppressing a differentiation into polymorphonuclear MDSCs (PMN-MDSCs). As a result, the increase in M-MDSCs contributes to the creation of an immunosuppressive TME, and the decrease in PMN-MDSCs suppresses angiogenesis, leading to an acquisition of resistance to chemotherapy. Accordingly, blockade of M-MDSC differentiation with an estrogen receptor inhibitor or anti-IL-34 monoclonal antibody suppressed M-MDSCs accumulation causing retardation of tumor growth and restores chemosensitivity of the tumor by promoting PMN-MDSCs accumulation. This

study demonstrates previously poorly understood mechanisms of MDSCs-mediated chemoresistance in the TME of TNBC, which is originated from the existence of IL-34, suggesting a new rationale for TNBC treatment.

KEYWORDS

Interleukin-34, Triple-negative breast cancer, Myeloid-derived suppressor cells, 4T1, Tumor microenvironment, Chemotherapy

STATEMENTS AND DECLARATIONS

Competing Interests

The authors declare no potential conflicts of interest

Funding information

This work was partly supported by Japan Agency for Medical Research and Development (AMED; Practical Research for Innovative Cancer Control), the Photo-excitonix Project, the project of junior scientist promotion in Hokkaido University (K. Seino), additionally, partly supported by JST SPRING (#JPMJSP2119, N. Kajihara), and JSPS KAKENHI (#22J21076, N. Kajihara).

Ethics approval and consent to participate

All animal procedures were approved by the Animal Care Committee of Hokkaido University (Approval number: 19-0094). All human clinical research was performed under the Declaration of Helsinki and was approved by the Clinical Research Administration Center of Hokkaido University Hospital (Registration number: 022-0009) and the Institutional Review Board of Osaka Rosai Hospital (Registration number: 31-18, 2020-41, 20210125). Informed consent was obtained from all individual subjects before tissue acquisition.

Authors' contributions

NK and KS designed the study. NK, TK, AH, SI, and JNK performed experiments. SI, TO, and MT obtained clinical samples. All authors analyzed data and discussed the results. NK, RO, and KS contributed to manuscript preparation. All authors approved the final version of this manuscript for publication.

INTRODUCTION

Breast cancer is the most common cancer and a major cause of cancer-related death among women worldwide.[1] It is reported that the average risk to develop breast cancer in normal women's life is as many as 12%.[2] According to Global Cancer Statistics 2020: GLOBOCAN 2020, the incidence and mortality of female breast cancer in 2020 worldwide were 2,261,419 new cases and 684,996 deaths, respectively.[1] Breast cancer is a highly heterogeneous disease with varying biological and clinical characteristics, which therefore makes treatment methods and disease prognosis diverse among subtypes. To distinguish the subtype of breast cancer, immunohistochemical (IHC) staining of breast cancer tumors is commonly used and can classify into four subtypes based on the expression of estrogen receptor (ER), progesterone receptor (PgR), and human epidermal growth factor receptor-related 2 (HER2). Among the subtypes, triple-negative breast cancer (TNBC) is characterized by the lack of these three receptors and accounts for 15-20% of all breast cancer.[3] TNBC typically shows a high degree of aggressiveness, poor prognosis, and a high rate of relapse.[4] Furthermore, it does not respond towards targeted treatment option except for surgery.[5] However, most TNBC patients are less susceptible to chemotherapy or become resistant to it during treatment.[6] Thus, chemoresistance is a critical problem that needs to be addressed for successful TNBC treatment.

In the past few decades, many studies have attempted to reveal the mechanism of inducing chemoresistance.[7][8][9] Most of them have emphasized the intrinsic ones, which occur inside cancer cells, such as apoptotic avoidance machinery or DNA repair mechanisms.[10][11] On the other hand, a lot of papers with recent advances have shown that extrinsic mechanisms are also important.[12][13] Its representative example is an interaction between tumor and immune cells within the tumor microenvironment (TME). The TME contains various immune system elements including myeloid cells, lymphocytes, and blood vessels. In particular, tumor-associated macrophages (TAMs) and myeloid-derived suppressor cells (MDSCs) constitute the dominant immune cell population in various tumors and play critical roles in multiple aspects of TME.[5][14] Importantly, an increase of TAMs and MDSCs infiltration into tumors is a hallmark of developing chemoresistance and correlates with poor prognosis.[15][16][17] Indeed, these myeloid cells in the TME are involved in many parts of pro-tumorigenic processes, including angiogenesis, immunosuppression, and tumor progression, and it is known that they are frequently observed in TNBC tumors.[5] However, the mechanism of TAMs- or MDSCs-mediated chemoresistance acquisition in TNBC has not been elucidated in detail.

Accumulating evidence has indicated that tumor-derived interleukin-34 (IL-34) can be a key molecule that causes chemoresistance.[4][18] Indeed, the importance of IL-

34 in chemoresistance is supported by the findings in a lung cancer study indicating that exposure of chemotherapeutic agents to cancer cells increases their production of IL-34.[19] In addition, IL-34 has been shown to induce immunosuppressive myeloid cells like TAMs and thus to be a possible linker between immunosuppressive TME and chemoresistance.[18][19][20] On the other hand, we have previously reported that IL-34 was expressed significantly higher and more frequently in TNBC than other breast cancer subtypes.[4] IL-34 was an independent poor prognosis factor in TNBC, and patients bearing IL-34 high-expressing TNBC showed a low survival rate.[4] From these data described above, it is anticipated that IL-34 may play an important role to induce chemoresistance in TNBC.

Based on these backgrounds, we have investigated the relationship between IL-34 and chemoresistance in TNBC. We firstly identified that, in TNBC tumors, IL-34 preferably induces MDSCs but not TAMs, and the IL-34-MDSCs axis contributes to chemoresistance. It is notable that blocking of IL-34 or MDSCs had a therapeutic potential to remedy the chemoresistance in TNBC. We here propose IL-34 as a molecular driver of chemoresistance in TNBC and suggest a novel therapeutic strategy.

MATERIALS AND METHODS

Cell lines

The TNBC cell line 4T1 was obtained from the American Type Culture Collection (ATCC) and cultured in RPMI-1640 (Fujifilm Wako Pure Chemical). Culture media was supplemented with 10% fetal bovine serum (FBS) (Sigma Aldrich), 100 U/ml penicillin (Nacalai Tesque), 100 μg/ml streptomycin (Nacalai Tesque), 0.1 mM MEM nonessential amino acids (Nacalai Tesque), and maintained at 37°C with 5% CO_2. Mycoplasma contamination of cell lines was checked using the MycoAlert™ Mycoplasma Detection Kit (Lonza), according to the manufacturer's instructions; no evidence of contamination was found.

Generation of IL-34 knockout (KO) cell line

IL-34 KO 4T1 cell line was generated using mIL-34 CRISPR/Cas9 KO plasmid (Santa Cruz Biotechnology). The plasmid was transfected into 2×10^6 cells using the Neon® Transfection System (Thermo Fisher Scientific), and the cells were incubated for 24 hours. After incubation, successful transfection of the plasmid was visually confirmed by the detection of green fluorescent protein (GFP) via fluorescent microscopy ObserverZ1 (Carl Zeiss AG). Plasmid-incorporated cells were selected by the GFP expression using

FACSAria cell sorter (BD Biosciences) 48 hours after transfection. Then, puromycin (2 μg/ml) was added to the medium and cultured for 48 hours to select the transfected cells.

Cell proliferation assay

Ctrl and IL-34 KO 4T1 cells (3×10^5) were seeded in 10 cm culture dishes. The number of cells was measured using a hemocytometer from day 1 to 3. When the cells were counted, they were stained with trypan blue, and the blue-stained cells were excluded from the total cell count.

Mouse experiments

Six to seven weeks old female BALB/c and MMTV-PyMT (FVB/N-Tg (MMTV-PyVT) 634Mul/J) mice were purchased from Japan SLC and The Jackson Laboratory, respectively. The mice were maintained under specific pathogen-free conditions and housed in 12 hours light/12 hours dark cycle in the animal facility at Hokkaido University. For *in vivo* assay, 1×10^5 4T1 cells were inoculated subcutaneously into the right flank of syngeneic female mice. Anti-IL-34 antibody (clone: C054-35) (200 μg/mouse), paclitaxel (PTX) (1.3 mg/kg), and/or methylpiperidino pyrazole (MPP) (1.0 mg/kg) were intraperitoneally (i.p.) administered when tumor size reached 5 mm in diameter. The anti-

IL-34 antibody, PTX, and MPP were purchased from BioLegend, Nippon Kayaku, and Cayman Chemical, respectively. Tumor size was measured by caliper three times a week. The 4T1 tumors were collected 14 days after the cell inoculation. Before the tumor recovery, for histological analysis and immunohistochemical (IHC) staining, mice underwent perfusion fixation. All animal experiments were approved by the Animal Care Committee of Hokkaido University (Approval number: 19-0094).

Isolation of tumor-infiltrating immune cells from solid tumor

According to the manufacturer's instructions, the isolation of tumor-infiltrating immune cells from solid tumors was performed by using BD Horizon Dri Tumor and Tissue Dissociation Reagent (BD Biosciences). The recovered tumor-infiltrating immune cells were analyzed by flow cytometry.

***In vitro* differentiation of bone marrow-derived MDSCs**

Bone marrow cells were isolated from the femora of female BALB/c mice and depleted of red blood cells with ACK lysis buffer. 1×10^6 bone marrow cells were cultured in 2 ml of RPMI-1640 culture media supplemented with 10% FBS, 100 U/ml penicillin, 100 μg/ml streptomycin, 50 ng/ml recombinant GM-CSF (BioLegend), with/without 50

ng/ml recombinant IL-34 (BioLegend). Cell cultures in 6-well plates were maintained at 37°C with 5% CO_2. Cells were collected on day 3 and analyzed by flow cytometry.

Collection of breast cancer patient-derived samples

For constructing human breast cancer organoids, we prepared breast cancer tissues obtained from breast cancer patients who underwent core needle biopsy under ultrasonographic guidance at Hokkaido University Hospital. For IHC examination of human TNBC tissues, 35 patients with Stages I–III TNBC were recruited retrospectively at Osaka Rosai Hospital, as previously described.[21] These patients underwent core needle biopsy under ultrasonographic guidance. Tumor biopsy samples were fixed in 10% buffered formaldehyde for histological analysis. Informed consent was obtained from all subjects before tissue acquisition, and organoid experiments and IHC examination utilizing patient-derived breast cancer tissues were approved by the Clinical Research Administration Center of Hokkaido University Hospital (Registration number: 022-0009) and the Institutional Review Board of Osaka Rosai Hospital (Registration number: 31-18, 2020-41, 20210125), respectively. All experiments utilizing human material were conducted according to the Declaration of Helsinki.

Histological analysis

The tumors were fixed in 4-10% Paraformaldehyde (Fujifilm Wako Pure Chemical) for 24 hours at 4°C. Tumors were dehydrated through 70-100% ethanol and immersed into xylene, then embedded in paraffin. The embedded samples were sliced, and 5 μm thick sections were obtained. For hematoxylin and eosin (H&E) staining, sections were deparaffinized, and immersed into H&E, then observed with a light microscope BX53F (Olympus).

IHC staining

Sections were deparaffinized, and endogenous peroxidase was blocked by 0.3 % H_2O_2 in distilled water for 20 minutes. For FOXP3 staining, antigen retrieval was performed for 1 minute by boiling the sections in citrate buffer. Sections were then incubated with BlockAce (DS Pharma Biomedical) in PBS for 1 hour to block non-specific reactions. After protein blocking, the mouse sections were incubated with rat anti-mouse CD4 (1:100, #13-9766-80, Thermo Fisher Scientific), FOXP3 (1:100, #14-5773-80, Thermo Fisher Scientific), CD31 (1:500, #550274, BD Pharmingen), or Gr-1 (1:200, #108401, BioLegend) antibody in PBS overnight at room temperature. Regarding the human sections, incubated with mouse anti-human IL-34 (1:4000, #MABT493, Sigma Aldrich),

FOXP3 (1:200, #14-4777-82, Thermo Fisher Scientific), CD14 (1:500, #75181, Cell Signaling Technology), CD15 (1:200, #555400, BD Pharmingen), or CD31 (1:1000, #11265-1-AP, Proteintech) antibody in PBS overnight at room temperature. Then, the sections were incubated with biotinylated donkey anti-rat/mouse IgG (Jackson ImmunoResearch) in PBS as the secondary antibody for 1 hour at room temperature, followed by incubation using an ABC Elite kit (Vector Laboratories) for 1 hour. Finally, the sections were incubated with 3, 3'-diaminobenzidine tetrahydrochloride (Fujifilm Wako Pure Chemical) in Tris-HCl containing H_2O_2 for 5-20 minutes and counterstained with hematoxylin. Sections were then enclosed using toluene. The observation was performed using a light microscope BX53F (Olympus).

Generation of human breast cancer organoids and IL-34 inhibitory experiment

Within 30 minutes of acquisition, breast tissue was minced, followed according to the manufacturer's instructions, and the isolation of tumor-infiltrating immune and cancer cells from solid tumors was performed by using BD Horizon Dri Tumor and Tissue Dissociation Reagent (BD Biosciences). Then, $1x10^5$ cells were resuspended in 50 µl of Matrigel, plated on the bottom of a 96-well plate, and solidified Matrigel. After Matrigel solidified, 200 µl of the organoid medium was added to each well and supplemented with

50 ng/ml recombinant human GM-CSF, IL-2, and IL-6 (BioLegend). Organoids in a 96-well plate were maintained at 37°C with 5% CO_2. Twelve hours after these manipulations, anti-IL-34 antibodies or control IgG were added to organoids, and MDSCs within the organoids were analyzed by flow cytometry on day 3.

Flow cytometry analysis and fluorescence-activated cell sorting

For extracellular staining, cells (2×10^5 cells/well) were blocked with FcR Blocking Reagent (TONBO biosciences) and stained the following molecules with antibodies or dye; CD3, CD4, CD14, CD15, CD45, CD86, CD115, CD11b, CD33, F4/80, Ly6C, and Ly6G (BioLegend), and 4', 6-diamidino-2-phenylindole (Cayman Chemical). For intracellular cytokine staining, cells were fixed and permeabilized with Cytofix/Cytoperm™ Buffer (BD Biosciences) after extracellular staining, then stained FOXP3 (BioLegend). Data were acquired using the FACSCelesta flow cytometer (BD Biosciences) and analyzed using FlowJo software (BD Biosciences). The gating strategies of immune cells are shown in Fig. S1. Cell sorting of tumor-infiltrating M-MDSCs and PMN-MDSCs was performed by FACSAria cell sorter (BD Biosciences). The antibodies used are summarized in Supplementary Table 1.

Quantitative polymerase chain reaction (qPCR)

Total RNA was extracted by using the TriPure Isolation Reagent (Roche). ReverTra Ace® qPCR RT Master Mix (Toyobo) was used to transcribe mRNA to cDNA. qPCR was performed on cDNA using specific primers and KAPA SYBR® FAST qPCR Master Mix (2x) ABI Prism® (Kapa Biosystems) on a StepOnePlus Real-Time PCR System (Thermo Fisher Scientific). Values were normalized to the expression of *Gapdh*. Relative expression levels were calculated using the 2-ddCt method. The primers are listed in Supplementary Table 2.

Clinical data analyses

Gene expression data and clinical data of IL-34 in the "Breast Invasive Carcinoma (TCGA, PanCancer Atlas)" dataset (N=1083) were obtained from www.cbioportal.org. We assigned these samples to breast cancer subtypes based on the PAM50 classification, and compared gene expression levels of IL-34, M-MDSC signature (CD274, NOS2, IL-10, VEGFA, CD14, TNF), PMN-MDSC signature (STAT1, STAT6, IRF1, ANXA1, LYZ, CXCL1, CXCL2, CXCR2, IL-8, LILRA3, TREM1, PTGS2, IL-4R, VEGFB, VEGFC, OLR1, CD244, LOX, SLC27A2), Treg cell signature (CD25), and vascular endothelial cell signature (CD31). Then we calculated the Spearman correlation coefficient and

generated the Kaplan-Meier survival curve. Data with missing survival information were excluded from this analysis.

Statistical analysis

Sample size and statistical tests are described in the figure legends. Every series of data are shown as mean ± SEM. A two-sided Student's *t*-test was used to compare between 2 groups. One-way ANOVA with Tukey's test was used to compare between 3 or more groups. The survival curves of the mice were determined using the Kaplan-Meier method, and the log-rank test was used for statistical evaluation. Pearson or Spearman correlation coefficient was used to examine the correlation between the two indicators. The p-value of < 0.05 was considered to be statistically significant. All statistical analyses were performed using JMP® 14 software (SAS Institute).

RESULTS

Tumor-derived IL-34 promotes tumor growth and orchestrates TME

We previously reported that IL-34 expression is elevated in human TNBC tumors and identified IL-34 as an independent poor prognostic factor for TNBC;[4] however, how IL-34 affects the TNBC's TME remains unknown. As an approach to identify the functions of IL-34 in the TME, we used a murine TNBC cell line 4T1. We first confirmed the effects of IL-34 on tumor growth using IL-34-producing and -deficient 4T1 (hereinafter referred to as control (Ctrl) and knockout (KO), respectively). Interestingly, Ctrl and KO cells proliferated equally *in vitro* (Fig. S2a), while KO cells showed significantly slower tumor growth compared to Ctrl cells in a subcutaneous transplantation model (Fig. 1a). At the time of tumor harvest, we confirmed that KO tumors weight showed marked reduction compared to Ctrl tumors (Fig. 1b). Furthermore, survival was prolonged in mice bearing KO tumors compared to Ctrl tumors (Fig. S2b). We then investigated how IL-34 promotes tumor growth *in vivo*. Based on previous reports that showed IL-34 enhances tumor growth by inducing TAMs,[18]-[20] we performed flow cytometry analysis of tumor-infiltrating immune cells to examine whether tumor-derived IL-34 increased them. However, there was no significant difference in the number of TAMs infiltrated into Ctrl and KO tumors, nor was a

309 difference in the number of T cells (Fig. 1c). On the other hand, the expression level of
310 CD86 on macrophages was significantly increased in KO tumors (Fig. 1d). It has been
311 reported that Treg cells can abrogate the T-cell activation capacity of antigen-presenting
312 cells (APCs) such as macrophages through down-regulating the CD86
313 expression.[22][23] Then, we examined the existence of Treg cells within the 4T1 tumors
314 and found that the number of them was drastically decreased in KO tumors compared to
315 Ctrl tumors (Fig. 1e and Fig. S3a, b).

316 We then explored whether the difference in Treg cells' infiltration was direct or
317 indirect effects by IL-34. Interestingly, we found that most Treg cells infiltrating into the
318 4T1 tumors expressed IL-34 receptor, colony-stimulating factor 1 receptor (CSF-1R) (Fig.
319 S3c), while its expression was barely observed in other tumor-infiltrating T cells (Fig.
320 S3d). To test whether IL-34 directly affects tumor-infiltrating Treg cells through binding
321 to CSF-1R, recombinant IL-34 was added to *in vitro* culture system that induces Treg
322 cells from naive T cells. However, notable change was not observed (data not shown),
323 suggesting that IL-34 does not directly affect the number of infiltrated Treg cells, although
324 they apparently express receptors for IL-34. We then set out to examine the possibility of
325 indirect pathways with which IL-34 changed the Treg cells infiltration. Treg cells are
326 known to be induced by intra-tumoral immunosuppressive myeloid cells such as TAMs

or MDSCs,[24][25] thus we focused on MDSCs because the infiltration of TAMs was not different between Ctrl and KO tumors. In consequence, there was a remarkable alteration in the MDSCs fraction infiltrated into each tumor (Fig. 1f). Two major subsets have been identified to compose MDSCs; one is monocytic MDSCs (M-MDSCs), which are similar to monocytes and are known to differentiate into tumor-associated macrophages (TAMs), and another one is polymorphonuclear MDSCs (PMN-MDSCs), which share phenotypic features with neutrophils.[26] In KO tumors, the population of $CD11b^{+}Ly6C^{+}Ly6G^{-}$ cells, representing M-MDSCs in mice, was decreased sharply compared with Ctrl tumors (Fig. 1f). Contrary, the population of $CD11b^{+}Ly6C^{lo}Ly6G^{+}$ cells, representing PMN-MDSCs in mice, was increased in KO tumors compared with Ctrl tumors (Fig. 1f). Because M-MDSCs are known to have a strong immunosuppressive ability and highly express CSF-1R,[27] these results suggest that IL-34 may promote *in vivo* tumor growth by affecting intra-tumoral M-MDSCs. Additionally, immunosuppressive effects via M-MDSCs are further supported by the results that M-MDSCs infiltrating in Ctrl tumors showed not only larger frequency but also a higher expression of *Ccl22*, which is critical for the migration of Treg cells, than M-MDSCs infiltrating in KO tumors (Fig. S3e).

The relationship between intra-tumoral IL-34 expression and MDSCs has not been well described. Thus, we examined the direct effect of IL-34 on the induction of

MDSCs by *in vitro* experiments. MDSCs were induced from bone marrow with granulocyte-macrophage colony-stimulating factor (GM-CSF) as previously described.[28] When recombinant IL-34 was added to the culture, a drastic increase in the induction of M-MDSCs was observed. On the other hand, PMN-MDSCs induction was slightly decreased (Fig. 2a). Of note, in human breast cancer patient-derived organoids, IL-34 inhibition slightly decreased M-MDSCs and increased PMN-MDSCs (Fig. S4a). To further consolidate the view that IL-34 affects MDSCs, we administered anti-IL-34 antibodies to MMTV-PyMT mice that spontaneously developed breast cancer. Thereby, an apparent decrease in M-MDSCs and an increase in PMN-MDSCs were observed in the TME of the IL-34 inhibitory group (Fig. S4b). In addition, accompanied by IL-34 inhibition-derived decrement of M-MDSCs, Treg cells also decreased (Fig. S4c). These data strongly suggest that IL-34 alters the balance of M-MDSCs and PMN-MDSCs. Collectively, these results support the notion that an increase of M-MDSCs (and a decrease of PMN-MDSCs) in Ctrl tumors is caused by tumor-derived IL-34, and the IL-34-MDSCs axis may enhance the tumor growth.

IL-34-MDSCs axis promotes tumor growth by creating an immunosuppressive TME

Although M-MDSCs have been reported to have a strong immunosuppressive ability,[27] the role of M-MDSCs in TNBC tumor growth has still been unidentified. To test the hypothesis that IL-34-induced M-MDSCs promote tumor growth, methylpiperidino pyrazole (MPP), an estrogen receptor inhibitor that can selectively deplete M-MDSCs,[29] was administered to the mice bearing Ctrl tumor. Administration of MPP resulted in significantly decreased growth of Ctrl tumors (Fig. 2b and Fig. S5a), along with a selective reduction of M-MDSCs in TME (Fig. 2c). The population of PMN-MDSCs, T cells, and macrophages did not change by the MPP administration (Fig. 2c and Fig. S5b), while, of note, a decrease of Treg cells was observed in the group with MPP treatment (Fig. S5c). These observations support the hypothesis that tumor-derived IL-34 induces M-MDSCs, which then recruits Treg cells to TME to support tumor growth by suppressing antitumor immune responses.

IL-34 lowers the therapeutic effect of chemotherapy via its effects on MDSCs

Given an immunosuppressive function of IL-34 in TME shown in our previous studies,[18]-[20] in addition to evidence regarding the relationship between chemoresistance and MDSCs,[17] we then explored the antitumor effect of paclitaxel (PTX), which is one of the standard treatments of TNBC, on *in vivo* tumor growth in the

381 presence or absence of IL-34. Interestingly, PTX exerted its therapeutic effect in KO but
382 not in Ctrl tumor-bearing mice (Fig. 3a-d). Since there was no significant change in the
383 immune cell component of TME with or without PTX treatment (Fig. S6a, b), a scenario
384 was suggested in which tumor-derived IL-34 limits the PTX's effect by regulating
385 MDSCs balance, namely, inducing M-MDSCs and suppressing PMN-MDSCs.

386 To verify the hypothesis that acquirement of chemoresistance is due to the IL-
387 34-MDSCs axis, combination therapy of PTX and MPP was performed for Ctrl tumors.
388 Consistent with the results shown in Fig. 2b, monotherapy of MPP delayed tumor growth,
389 and administration of PTX combined with MPP showed a synergistic antitumor effect
390 (Fig. 3e and Fig. S6c). These results suggest that the antitumor effect by the combination
391 therapy with PTX and MPP was mediated by an alteration of MDSCs' balance in the
392 TME that occurred by the administration of MPP. In fact, TME analysis exhibited a
393 decrease in M-MDSCs and a contrasting increase in PMN-MDSCs in the MPP-treated
394 and MPP/PTX combination therapy groups compared to the PTX monotherapy group
395 (Fig. 3f and Fig. S6d). Taken together, the above observations are indicative of a negative
396 involvement of the IL-34-MDSCs axis in the therapeutic effect of chemotherapy.

397

398 **IL-34-MDSCs axis dramatically suppresses angiogenesis and forms a**

chemoresistant tumor

We next asked how the IL-34-MDSCs axis limits the therapeutic effect of chemotherapy. To address this issue, we evaluated the vascular invasion into the tumors, which has been reported as a representative mechanism for chemoresistance caused by MDSCs.[30][31][32] Of note, blood vessels did not invade the central part of the Ctrl tumors and were observed only in the outer layer. Conversely, massive invasion of blood vessels into the central part was observed in KO tumors (Fig. 4a). In addition to the clear difference of blood vessel distribution between the two tumors represented by the histological images, quantification of vascular endothelial cells revealed their dramatic increase in KO tumors compared to Ctrl tumors (Fig. 4a).

We then investigated the angiogenic ability of MDSCs in the tumors, mainly focusing on PMN-MDSCs that increased in KO tumors. Interestingly, PMN-MDSCs isolated from Ctrl tumors showed a marked reduction of *Vegfa* and *Vegfb* expression levels compared to those from KO tumors (Fig. 4b), and similar trends were observed for M-MDSCs (Fig. S7a). The levels of these factors were not different between Ctrl and KO tumor cells (Fig. S7b). These results suggest that the IL-34-MDSCs axis suppresses angiogenesis and then causes chemoresistance through inhibiting chemotherapeutic agents from reaching the entire tumor. In fact, many MDSCs (Gr-1$^+$ cells) that can induce

417 angiogenesis invaded the central part of KO tumors, whereas, in Ctrl tumors, their
418 invasion was observed only in the outer layer (Fig. 4c). Collectively, the above
419 observations suggest that tumor-derived IL-34 acts on MDSCs to create an
420 immunosuppressive and chemoresistant TME.
421
422 **IL-34 blockade restores chemoresistance *in vivo***
423 To gain further understanding of IL-34's effect on MDSCs in the TME, we next examined
424 whether IL-34 inhibiting reagents affected chemoresistance. Administration of an anti-
425 IL-34 antibody led to a significant increase in the density of blood vessels within the
426 tumors, accompanied by an increasing trend of PMN-MDSCs (Fig. 5a and Fig. S8a). This
427 result suggests that the IL-34 blockade may restore the penetration of chemotherapeutic
428 agents. In addition, IL-34 inhibition tended to decrease the frequency of M-MDSCs and
429 Treg cells in the TME (Fig. S8b), suggesting that the immunosuppressive circumstance
430 in the TME of Ctrl tumors was also improved by the IL-34 blockade.
431 We finally treated Ctrl tumors with a combination of IL-34 blockade and PTX.
432 Although Ctrl tumors has not sensitive to PTX (Fig. 3a, b), this combinatory treatment
433 induced significant growth retardation (Fig. 5b). These results demonstrate that the
434 efficacy of PTX could be restored by targeting the IL-34-MDSCs axis. Notably, the above

results further illustrate that tumor-derived IL-34 indeed contributes to chemoresistance *in vivo*. Moreover, the combination therapy of PTX and IL-34 inhibition was accompanied by a decrease in M-MDSCs (Fig. 5c), suggesting that this therapy could induce weaning from immunosuppressive TME. In fact, an increase in T cells and TAMs was observed in the combination therapy group compared to the PTX monotherapy group (Fig. S8c). Considering that chemotherapy is originally used to induce cell death in tumors and augment immune responses to cancer, the above findings may have an implication for developing future chemotherapy because most tumors show certain levels of resistance against chemotherapy.

Involvement of IL-34-MDSCs axis in human TNBC

To assess whether the findings obtained in our mouse experiments can be extrapolated to human TNBC's TME, we analyzed human data from The Cancer Genome Atlas (TCGA). This analysis revealed that there was a positive correlation between IL-34 expression in human TNBC tumors and intra-tumoral M-MDSCs (Fig. 6a). Furthermore, we found that intra-tumoral M-MDSCs positively correlated with intra-tumoral Treg cells (Fig. 6b), suggesting that immunosuppressive TME through the IL-34-MDSCs axis is also established in human TNBC. In fact, consistent with our mouse experiments (Fig. 1f and

Fig. S2b), high IL-34 expression and high M-MDSCs infiltration in human TNBC tumors showed worse patient survival (Fig. 6c). Hence, when we then analyzed the relationship between intra-tumoral IL-34 expression and PMN-MDSCs by using SLC27A2, a marker of human PMN-MDSCs,[33] expression levels of IL-34 and SLC27A2 were negatively correlated (Fig. 6d). In addition, there was a positive correlation between intra-tumoral PMN-MDSCs and vascular endothelial cells (Fig. 6e), which supports our results obtained in the mouse experiments (Fig. 4, 5).

Finally, we confirmed if the results from gene expression analyses of the TCGA dataset are consistent with protein expression in TNBC tissues, using the IHC examination for each candidate molecule (Fig. S9a). Of note, within the TNBC tissues, IL-34 expression positively correlated with M-MDSC infiltration, and moreover, M-MDSCs and Treg cells infiltration also related positively. On the other hand, despite no relation between IL-34 expression and PMN-MDSCs infiltration in the TNBC cohort used in the present study, the infiltration of PMN-MDSCs showed a strong and positive association with vascular endothelial cells' invasion in the TNBC tumors (Fig. S9b).

Collectively, the mouse data in this study overall represent the pathological situation of human TNBC's TME, suggesting that IL-34-targeted therapy may derepress immunosuppression and increase the effectiveness of chemotherapy in TNBC. However,

471 there are some exceptions due to the complex composition of TME in TNBC patients, as
472 the relationship between IL-34 and PMN-MDSCs indicated at last, and further studies in
473 large cohorts are needed.
474

DISCUSSION

We turn our eyes to previous research regarding IL-34 and cancer; in esophageal cancer, it has been reported that IL-34 expression in chemotherapy-nonresponsive patients was significantly higher than that in chemotherapy-responsive patients.[34] IL-34 expression converts the TME toward a TAM-rich immunosuppressive one resulting in a chemoresistance and worse prognosis in IL-34-high expressing patients.[34] In also lung cancer, we previously demonstrated that chemoresistant tumor-derived IL-34 enhanced local immunosuppressive degree by inducing TAMs from monocytes via paracrine pathways and promoted chemoresistant cancer cells' survival via autocrine pathways.[19] In addition, we indicated that both existences of high IL-34 expression and high TAM infiltration in TME were associated with worse progression-free survival in an ovarian cancer study.[18] Similar results have been documented in also colorectal cancer.[35] Thus, IL-34 induces immunosuppressive TAMs within the TME, leading to therapeutic resistance and poor outcomes in various cancers.

While studies regarding IL-34 and cancer have hitherto exhibited the TAMs-mediated dynamics by IL-34 in TME, in this study, we have demonstrated for the first time that TNBC tumor-derived IL-34 functions as an MDSCs balance regulator; namely, it induces differentiation of M-MDSCs from the bone marrow and in turn suppresses

differentiation of PMN-MDSCs. As IL-34 has been so far reported as a TAMs-mediated immunosuppressive factor rather than an MDSC inducer, our findings provide new insights into how IL-34 contributes to the regulation of immune response within TME.

The induction of MDSCs is an important immune-evading mechanism elicited by tumors. Intra-tumoral M-MDSCs, in particular, are more potent immunosuppressors than PMN-MDSCs,[27] and indeed, a previous human study showed that the number of M-MDSCs but not of PMN-MDSCs correlated directly with antitumor T cell suppression.[36] In addition to their intrinsic immunosuppressive ability, M-MDSCs indirectly attenuate immune response by recruiting Treg cells via CCL22 production in TME.[37] Our results indicated that IL-34 strongly triggers this pathway, orchestrates MDSCs (increases M-MDSC) to create the immunosuppressive TME, and consequently promotes tumor growth. In contrast, the resulting decrease of PMN-MDSCs could negatively regulate angiogenesis in TME, making it difficult for chemotherapeutic agents to reach the entire tumor. Therefore, IL-34, which regulates the balance of these two types of MDSCs, is a crucial factor in controlling TME.

The relationship between angiogenesis and tumor malignancy has been discussed in many studies.[30][31][32] In general, angiogenesis is an event that promotes tumor growth;[30] however, it has advantages in terms of drug delivery that allows

511 antitumor drugs to penetrate tumors.[38] In fact, our results have consistently indicated
512 dramatic positive effects of chemotherapy for blood vessel-rich tumors. Moreover, tumor-
513 infiltrated immune cell analyses revealed much infiltration of PMN-MDSCs in
514 chemotherapy-susceptible tumors, which contained much vascular structure.

515 One of the most common and well-studied mechanisms inducing angiogenesis
516 is the production of VEGF by MDSCs.[30][31] VEGF is a growth factor secreted by
517 various cells and plays an important role in the general process of angiogenesis.[39]
518 Considering our results based on these backgrounds, it is worth noting that many PMN-
519 MDSCs infiltrated into IL-34-deficient tumors in which many blood vessels were
520 observed. In fact, a previous study has shown that co-injection of tumor-derived PMN-
521 MDSCs and tumor cells exhibit significantly higher intra-tumoral vascular density than
522 mice injected with tumor cells alone.[32] In short, PMN-MDSCs have a strong ability to
523 contribute to tumor angiogenesis, which increment may lead to a dramatic increase of
524 vasculature within IL-34-deficient tumors.

525 In addition to the quantitative changes in PMN-MDSCs, the MDSCs isolated
526 from IL-34-deficient tumors displayed remarkably increased *Vegfa* and *Vegfb* expression
527 levels compared to those isolated from IL-34-producing tumors. These observations
528 suggest that tumor-derived IL-34 may contribute to the suppression of VEGF expression

through regulating downstream signaling of CSF-1R. Similarly, we have previously shown that IL-34-deficient tumors are IL-6-rich,[4] which may stimulate MDSCs via activation of the STAT3-mediated pathway.[40] This activation may induce more VEGF production by MDSCs, probably establishing a positive feedback loop that sustains their angiogenic activity.[41] These observations overall support the notion that PMN-MDSCs infiltrating into IL-34-deficient tumors are a promoting factor for angiogenesis. In addition, administration of anti-IL-34 antibody to IL-34-producing tumors increased the frequency of intra-tumoral PMN-MDSCs and resulted in increased neo-angiogenesis. Collectively, the IL-34-MDSCs axis in tumors seems to play a major role in angiogenic suppression and contribute to chemoresistance.

TNBC is a subtype of breast cancer with the worst susceptibility to anti-tumor treatment, including chemotherapy. It has been demonstrated that TNBC shows various levels of chemoresistance via different mechanisms.[6] We have indicated that IL-34 is characteristically expressed in TNBC and acts as an essential factor for chemoresistance. In this study, we have shown for the first time a novel mechanism regulating intra-tumoral MDSCs by IL-34, which then affected Treg infiltration and angiogenesis. Our study may provide insights on how to manipulate the immune system in TNBC to enhance the effectiveness of chemotherapeutic agents. Indeed, our data demonstrating that the

547 combination therapy of IL-34 blockade and chemotherapeutic agents was very effective

548 could be clinically significant.

549

REFERENCES

1. Sung H, Ferlay J, Siegel RL, Laversanne M, Soerjomataram I, Jemal A, et al. Global Cancer Statistics 2020: GLOBOCAN Estimates of Incidence and Mortality Worldwide for 36 Cancers in 185 Countries. CA Cancer J Clin. 2021;71:209–49.

2. Liu Y, Qiu N, Shen L, Liu Q, Zhang J, Cheng YY, et al. Nanocarrier-mediated immunogenic chemotherapy for triple negative breast cancer. J Control Release. 2020;323:431–41.

3. Keenan TE, Tolaney SM. Role of immunotherapy in triple-negative breast cancer. JNCCN J Natl Compr Cancer Netw. 2020;18:479–89.

4. Kajihara N, Kitagawa F, Kobayashi T, Wada H, Otsuka R, Seino K ichiro. Interleukin-34 contributes to poor prognosis in triple-negative breast cancer. Breast Cancer. 2020;27:1198–204.

5. Cha YJ, Koo JS. Role of Tumor-Associated Myeloid Cells in Breast Cancer. Cells. 2020;9:1785.

6. Nedeljković M, Damjanović A. Mechanisms of Chemotherapy Resistance in Triple-Negative Breast Cancer-How We Can Rise to the Challenge. Cells. 2019;8:957.

7. Zheng X, Carstens JL, Kim J, Scheible M, Kaye J, Sugimoto H, et al. Epithelial-to-mesenchymal transition is dispensable for metastasis but induces chemoresistance in

568 pancreatic cancer. Nature. 2015;527:525–30.

569 8. Patch AM, Christie EL, Etemadmoghadam D, Garsed DW, George J, Fereday S, et

570 al. Whole-genome characterization of chemoresistant ovarian cancer. Nature.

571 2015;521:489–94.

572 9. Low HB, Wong ZL, Wu B, Kong LR, Png CW, Cho YL, et al. DUSP16 promotes

573 cancer chemoresistance through regulation of mitochondria-mediated cell death. Nat

574 Commun. 2021;12:2284.

575 10. Wilson TR, Longley DB, Johnston PG. Chemoresistance in solid tumours. Ann

576 Oncol. 2006;17:315–24.

577 11. Holohan C, Van Schaeybroeck S, Longley DB, Johnston PG. Cancer drug

578 resistance: An evolving paradigm. Nat Rev Cancer. 2013;13:714–26.

579 12. Karin M, Cao Y, Greten FR, Li ZW. NF-κB in cancer: From innocent bystander to

580 major culprit. Nat Rev Cancer. 2002;2:301–10.

581 13. Pardoll DM. The blockade of immune checkpoints in cancer immunotherapy. Nat

582 Rev Cancer. 2012;12:252–64.

583 14. Veglia F, Sanseviero E, Gabrilovich DI. Myeloid-derived suppressor cells in the era

584 of increasing myeloid cell diversity. Nat Rev Immunol. 2021;21:485–98.

585 15. Noy R, Pollard JW. Tumor-Associated Macrophages: From Mechanisms to

586 Therapy. Immunity. 2014;41:49–61.

587 16. Ruffell B, Coussens LM. Macrophages and therapeutic resistance in cancer. Cancer

588 Cell. 2015;27:462–72.

589 17. Anestakis D, Petanidis S, Domvri K, Tsavlis D, Zarogoulidis P, Katopodi T.

590 Carboplatin chemoresistance is associated with CD11b+/Ly6C+ myeloid release and

591 upregulation of TIGIT and LAG3/CD160 exhausted T cells. Mol Immunol.

592 2020;118:99–109.

593 18. Endo H, Hama N, Baghdadi M, Ishikawa K, Otsuka R, Wada H, et al. Interleukin-

594 34 expression in ovarian cancer: A possible correlation with disease progression. Int

595 Immunol. 2019;32:175–86.

596 19. Baghdadi M, Wada H, Nakanishi S, Abe H, Han N, Putra WE, et al. Chemotherapy-

597 Induced IL34 Enhances Immunosuppression by Tumor-Associated Macrophages and

598 Mediates Survival of Chemoresistant Lung Cancer Cells. Cancer Res. 2016;76:6030–

599 42.

600 20. Hama N, Kobayashi T, Han N, Kitagawa F, Kajihara N, Otsuka R, et al. Interleukin-

601 34 Limits the Therapeutic Effects of Immune Checkpoint Blockade. iScience.

602 2020;23:101584.

603 21. Imanishi S, Morishima H, Gotoh T. Significance of the effects of chemotherapy on

programmed death-ligand 1 expression in triple-negative breast cancer. Jpn J Clin Oncol. 2022;31:S324.

22. Cederbom L, Hall H, Ivars F. CD4+CD25+ regulatory T cells down-regulate co-stimulatory molecules on antigen-presenting cells. Eur J Immunol. 2000;30:1538–43.

23. Gu P, Fang Gao J, D'Souza CA, Kowalczyk A, Chou KY, Zhang L. Trogocytosis of CD80 and CD86 by induced regulatory T cells. Cell Mol Immunol. 2012;9:136–46.

24. de Haas N, de Koning C, Spilgies L, de Vries IJM, Hato S V. Improving cancer immunotherapy by targeting the STATe of MDSCs. Oncoimmunology. 2016;5:1–11.

25. Pan Y, Yu Y, Wang X, Zhang T. Tumor-Associated Macrophages in Tumor Immunity. Front Immunol. 2020;11:583084.

26. Kumar V, Patel S, Tcyganov E, Gabrilovich DI. The Nature of Myeloid-Derived Suppressor Cells in the Tumor Microenvironment. Trends Immunol. 2016;37:208–20.

27. Gabrilovich DI, Ostrand-Rosenberg S, Bronte V. Coordinated regulation of myeloid cells by tumours. Nat Rev Immunol. 2012;12:253–68.

28. Höchst B, Mikulec J, Baccega T, Metzger C, Welz M, Peusquens J, et al. Differential induction of Ly6G and Ly6C positive myeloid derived suppressor cells in chronic kidney and liver inflammation and fibrosis. PLoS One. 2015;10:1–13.

29. Svoronos N, Perales-Puchalt A, Allegrezza MJ, Rutkowski MR, Payne KK, Tesone

622 AJ, et al. Tumor cell–independent estrogen signaling drives disease progression through
623 mobilization of myeloid-derived suppressor cells. Cancer Discov. 2017;7:72–85.
624 30. Finke J, Ko J, Rini B, Rayman P, Ireland J, Cohen P. MDSC as a mechanism of
625 tumor escape from sunitinib mediated anti-angiogenic therapy. Int Immunopharmacol.
626 2011;11:856–61.
627 31. Vetsika E, Koukos A, Kotsakis A. Myeloid-Derived Suppressor Cells: Major
628 Figures that Shape the Immunosuppressive and Angiogenic Network in Cancer. Cells.
629 2019;8:1647.
630 32. Yang L, DeBusk LM, Fukuda K, Fingleton B, Green-Jarvis B, Shyr Y, et al.
631 Expansion of myeloid immune suppressor Gr+CD11b+ cells in tumor-bearing host
632 directly promotes tumor angiogenesis. Cancer Cell. 2004;6:409–21.
633 33. Veglia F, Tyurin VA, Blasi M, De Leo A, Kossenkov A V., Donthireddy L, et al.
634 Fatty acid transport protein 2 reprograms neutrophils in cancer. Nature. 2019;569:73–8.
635 34. Nakajima S, Mimura K, Saito K, Thar Min AK, Endo E, Yamada L, et al.
636 Neoadjuvant chemotherapy induces IL34 signaling and promotes chemoresistance via
637 tumor-associated macrophage polarization in esophageal squamous cell carcinoma. Mol
638 Cancer Res. 2021;19:1085–95.
639 35. Kobayashi T, Baghdadi M, Han N, Murata T, Hama N, Otsuka R, et al. Prognostic

640 value of IL-34 in colorectal cancer patients. Immunol Med. 2019;42:169–75.

641 36. Mandruzzato S, Solito S, Falisi E, Francescato S, Chiarion-Sileni V, Mocellin S, et

642 al. IL4Rα + Myeloid-Derived Suppressor Cell Expansion in Cancer Patients . J

643 Immunol. 2009;182:6562–8.

644 37. Yang Y, Li C, Liu T, Dai X, Bazhin A V. Myeloid-Derived Suppressor Cells in

645 Tumors: From Mechanisms to Antigen Specificity and Microenvironmental Regulation.

646 Front Immunol. 2020;11:1–22.

647 38. Dass CR. Tumour angiogenesis, vascular biology and enhanced drug delivery. J

648 Drug Target. 2004;12:245–55.

649 39. Hicklin DJ, Ellis LM. Role of the vascular endothelial growth factor pathway in

650 tumor growth and angiogenesis. J Clin Oncol. 2005;23:1011–27.

651 40. Kitamura H, Ohno Y, Toyoshima Y, Ohtake J, Homma S, Kawamura H, et al.

652 Interleukin-6/STAT3 signaling as a promising target to improve the efficacy of cancer

653 immunotherapy. Cancer Sci. 2017;108:1947–52.

654 41. Chen Z, Zhong CH. STAT3: A critical transcription activator in angiogenesis. Med

655 Res Rev. 2008;28:185–200.

656

657

FIGURE LEGENDS

Fig. 1 IL-34 promotes in vivo tumor growth by modulating TME in TNBC.

(a) Subcutaneous tumor growth in BALB/c mice inoculated with control (Ctrl) and IL-34 knockout (KO) 4T1 cells (1 x 10^5 cells, n=6). Similar results were obtained in several independent experiments. (b) Bar graphs representing tumor weight of harvested Ctrl and IL-34 KO 4T1 tumors at 14 days post tumor inoculation (n=6). (c) Bar graphs representing the frequency of TAM ($CD11b^+F4/80^+$ cells) and T cell ($CD3^+$ cells) within $CD45^+$ cells infiltrated in the tumors described in Fig. 1a (n=6). (d) Representative histograms indicated for Ctrl (Blue), KO (red), and isotype (gray) (left) and mean fluorescence intensity (MFI) (right) of CD86 expression on $CD86^+$ TAM ($CD45^+CD11b^+F4/80^+CD86^+$ cells) infiltrated in the tumors described in Fig. 1a (n=6). (e) Representative IHC staining of CD4 (brown) and FOXP3 (black) in Ctrl and IL-34 KO 4T1 tumors at the time of day 14 from tumor inoculation (left). Scale bars=50 μm. Quantification of $CD4^+FOXP3^+$ cells in Ctrl and KO tumors from a field of view (n=3, right). (f) Representative plots of M-MDSC ($CD11b^+Ly6C^+Ly6G^-$ cells) and PMN-MDSC ($CD11b^+Ly6C^{lo}Ly6G^+$ cells) (left). Bar graphs representing the frequency of M-MDSC and PMN-MDSC within $CD45^+$ cells infiltrated in the tumors described in Fig. 1a (n=6, right). Values were analyzed by a two-sided Student's *t*-test (a-f) and are shown

as mean ± SEM. Asterisk indicates a significant difference; *p<0.05, **p<0.01, ***p<0.001, compared with the control group.

Fig. 2 IL-34 creates an immunosuppressive TME via induction of M-MDSCs in TNBC.

(a) In vitro induction assay of MDSCs from bone marrow in the presence or absence of IL-34. Bar graphs representing the frequency of M-MDSC ($CD11b^{+}Ly6C^{+}Ly6G^{-}$ cells) and PMN-MDSC ($CD11b^{+}Ly6C^{lo}Ly6G^{+}$ cells) within $CD45^{+}$ cells differentiated from bone marrow (n=3). (b) Subcutaneous tumor growth in BALB/c mice inoculated with Ctrl and IL-34 KO 4T1 cells (1 x 10^5 cells, n=4-8). Methylpiperidino pyrazole (MPP) (1.0 mg/kg) or control DMSO was administered intraperitoneally daily for 5-14 days. (c) Representative plots of M-MDSC ($CD11b^{+}Ly6C^{+}Ly6G^{-}$ cells) and PMN-MDSC ($CD11b^{+}Ly6C^{lo}Ly6G^{+}$ cells) (top). Bar graphs representing the frequency of M-MDSC and PMN-MDSC within $CD45^{+}$ cells infiltrated in the tumors described in Fig. 2b (n=4-8, bottom). Values were analyzed by a two-sided Student's *t*-test (a) and one-way ANOVA with Tukey's test (b-c) and are shown as mean ± SEM. Asterisk indicates a significant difference; *p<0.05, ***p<0.001, compared with the control group.

Fig. 3 IL-34-MDSCs axis negates the antitumor effects of Paclitaxel (PTX) in TNBC. (a) Subcutaneous tumor growth in BALB/c mice inoculated with Ctrl 4T1 cells (1 x 10^5 cells, n=6). PTX (1.3 mg/kg) or control saline was administered intraperitoneally daily for 5-14 days. (b) Bar graphs representing tumor weight of harvested Ctrl 4T1 tumors at 14 days post tumor inoculation (n=6). (c) Subcutaneous tumor growth in BALB/c mice inoculated with IL-34 KO 4T1 cells (1 x 10^5 cells, n=6). PTX (1.3 mg/kg) or control Saline was administered intraperitoneally daily for 5-14 days. (d) Bar graphs representing tumor weight of harvested IL-34 KO 4T1 tumors at 14 days post tumor inoculation (n=6). (e) Subcutaneous tumor growth in BALB/c mice inoculated with Ctrl 4T1 cells (1 x 10^5 cells, n=12). PTX (1.3 mg/kg), control Saline, MPP (1.0 mg/kg), control DMSO, or their combination was administered intraperitoneally daily for 5-14 days. (f) Bar graphs representing the frequency of M-MDSC ($CD11b^+Ly6C^+Ly6G^-$ cells) and PMN-MDSC ($CD11b^+Ly6C^{lo}Ly6G^+$ cells) within $CD45^+$ cells infiltrated in the tumors described in Fig. 3e (n=12). Values were analyzed by a two-sided Student's *t*-test (a-d) and one-way ANOVA with Tukey's test (e-f) and are shown as mean ± SEM. Asterisk indicates a significant difference; *p<0.05, **p<0.01, ***p<0.001, compared with the control group.

Fig. 4 IL-34-MDSCs axis has the potential to suppress angiogenesis.

(a) Ctrl and IL-34 KO 4T1 cells (1 x 10^5 cells) were subcutaneously inoculated into BALB/c mice. Representative IHC staining of CD31 (brown) in Ctrl and IL-34 KO 4T1 tumors at the time of day 14 from tumor inoculation (left). Scale bars=200 μm. Quantification of $CD31^+$ cells in Ctrl and IL-34 KO 4T1 tumors from a field of view (n=3, right). (b) PMN-MDSCs were sorted from cell suspensions of tumor-infiltrated immune cells at the time of day 14 from tumor inoculation. Bar graphs representing fold induction of *Vegfa* and *Vegfb* expression of PMN-MDSCs in Ctrl and IL-34 KO 4T1 tumors (n=3). Gene expression levels were determined by RT-PCR, as normalized to *Gapdh*. (c) Representative IHC staining of Gr-1 (brown) in Ctrl and IL-34 KO 4T1 tumors at the time of day 14 from tumor inoculation. Scale bars=100 μm. Values were analyzed by a two-sided Student's *t*-test (a-b) and are shown as mean ± SEM. Asterisk indicates a significant difference; **p<0.01, ***p<0.001, compared with the control group.

Fig. 5 Effects of IL-34 blockade on chemoresistance including in vivo tumor growth and TME.

(a) Ctrl 4T1 cells (1 x 10^5 cells) were subcutaneously inoculated into BALB/c mice. Anti-IL-34 antibody (200 μg) or control IgG was administered intraperitoneally daily for 5-14

730 days. Representative IHC staining of CD31 (brown) in Ctrl 4T1 tumors treated
731 with/without αIL-34 at the time of day 14 from tumor inoculation (left). Scale bars=200
732 μm. Quantification of $CD31^+$ cells in Ctrl 4T1 tumors treated with/without αIL-34 from
733 a field of view (n=3, right). (b) Subcutaneous tumor growth in BALB/c mice inoculated
734 with Ctrl 4T1 cells (1 x 10^5 cells, n=12). PTX (1.3 mg/kg), anti-IL-34 antibody (200 μg),
735 control saline, control IgG, or their combination was administered intraperitoneally daily
736 for 5-14 days. (c) Bar graphs representing the frequency of M-MDSC
737 ($CD11b^+Ly6C^+Ly6G^-$ cells) and PMN-MDSC ($CD11b^+Ly6C^{lo}Ly6G^+$ cells) within
738 $CD45^+$ cells infiltrated in the tumors described in Fig. 5b (n=12). Values were analyzed
739 by a two-sided Student's *t*-test (a) and one-way ANOVA with Tukey's test (b-c) and are
740 shown as mean ± SEM. Asterisk indicates a significant difference; *$p<0.05$, **$p<0.01$,
741 compared with the control group.
742
743 **Fig. 6 Potential involvement of IL-34-MDSCs axis in human TNBC.**
744 (a) Pearson correlation coefficient between relative IL-34 expression in tumors and intra-
745 tumoral M-MDSCs infiltration is shown. (b) Pearson correlation coefficient between
746 intra-tumoral Treg cells infiltration and intra-tumoral M-MDSCs infiltration is shown. (c)
747 Kaplan-Meier plot of overall survival of TNBC patients with high IL-34 expression/high

M-MDSCs infiltration and low IL-34 expression/low M-MDSCs infiltration stratified by PAM50 subtype. Values were analyzed by a Log-rank test. (d) Spearman correlation coefficient between relative IL-34 expression in tumors and intra-tumoral PMN-MDSCs infiltration is shown. (e) Pearson correlation coefficient between intra-tumoral vascular endothelial cells infiltration and intra-tumoral PMN-MDSCs infiltration is shown.

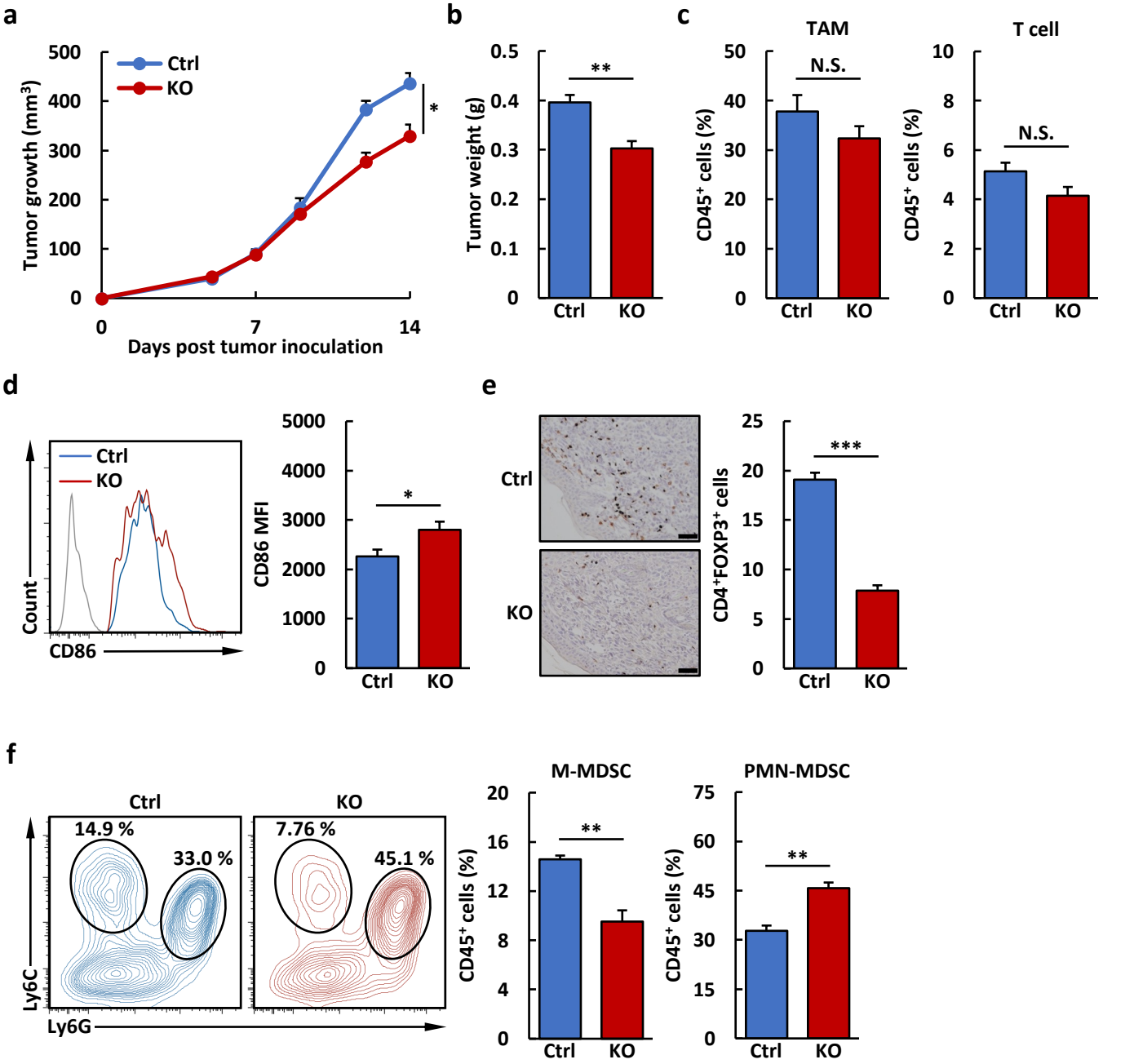

Fig. 1 IL-34 promotes in vivo tumor growth by modulating TME in TNBC.
(a) Subcutaneous tumor growth in BALB/c mice inoculated with control (Ctrl) and IL-34 knockout (KO) 4T1 cells (1×10^5 cells, n=6). Similar results were obtained in several independent experiments. (b) Bar graphs representing tumor weight of harvested Ctrl and IL-34 KO 4T1 tumors at 14 days post tumor inoculation (n=6). (c) Bar graphs representing the frequency of TAM ($CD11b^+F4/80^+$ cells) and T cell ($CD3^+$ cells) within $CD45^+$ cells infiltrated in the tumors described in Fig. 1a (n=6). (d) Representative histograms indicated for Ctrl (Blue), KO (red), and isotype (gray) (left) and mean fluorescence intensity (MFI) (right) of CD86 expression on $CD86^+$ TAM ($CD45^+CD11b^+F4/80^+CD86^+$ cells) infiltrated in the tumors described in Fig. 1a (n=6). (e) Representative IHC staining of CD4 (brown) and FOXP3 (black) in Ctrl and IL-34 KO 4T1 tumors at the time of day 14 from tumor inoculation (left). Scale bars=50 μm. Quantification of $CD4^+FOXP3^+$ cells in Ctrl and KO tumors from a field of view (n=3, right). (f) Representative plots of M-MDSC ($CD11b^+Ly6C^+Ly6G^-$ cells) and PMN-MDSC ($CD11b^+Ly6C^{lo}Ly6G^+$ cells) (left). Bar graphs representing the frequency of M-MDSC and PMN-MDSC within $CD45^+$ cells infiltrated in the tumors described in Fig. 1a (n=6, right). Values were analyzed by a two-sided Student's *t*-test (a-f) and are shown as mean ± SEM. Asterisk indicates a significant difference; *p<0.05, **p<0.01, ***p<0.001, compared with the control group.

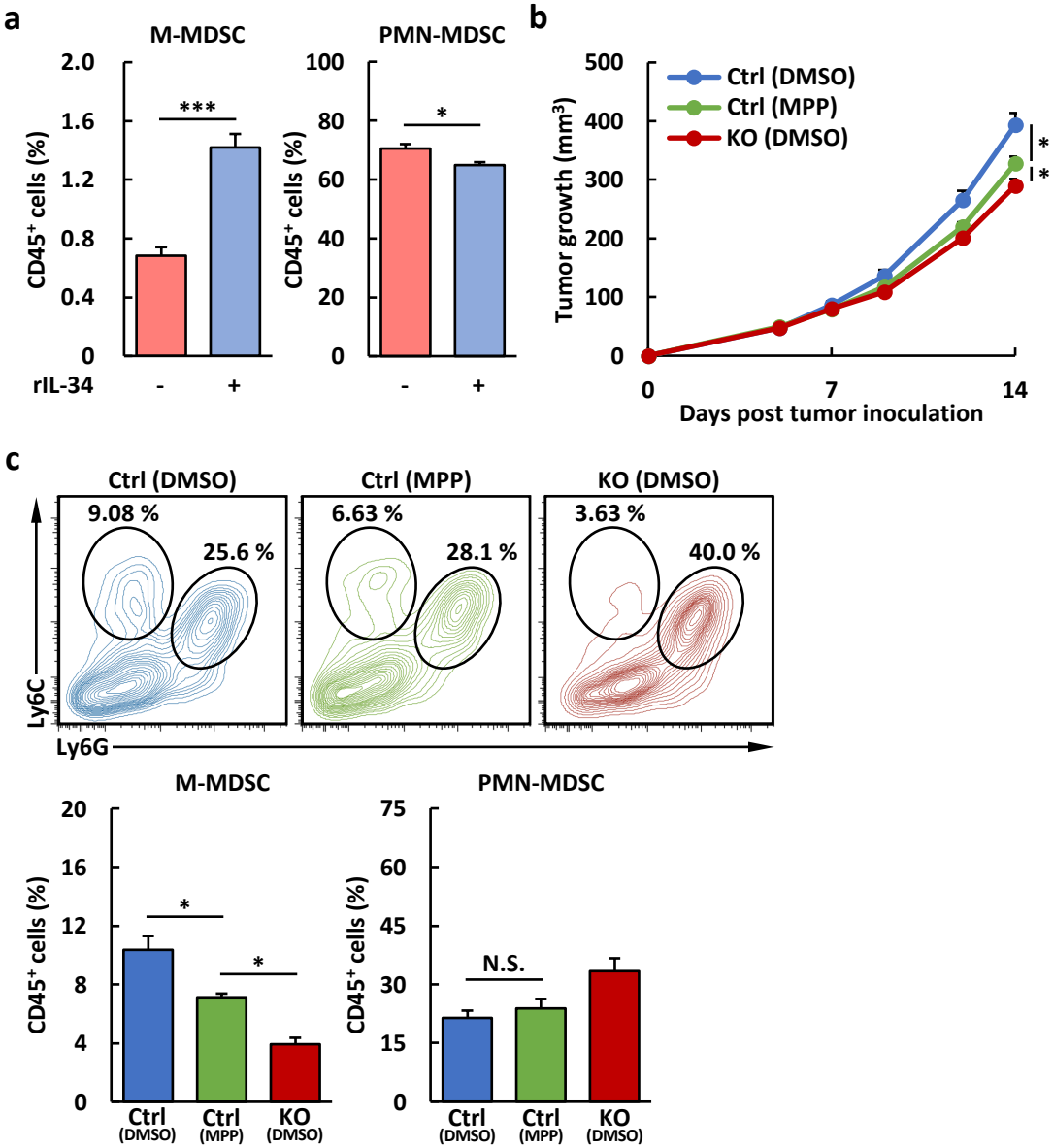

Fig. 2 IL-34 creates an immunosuppressive TME via induction of M-MDSCs in TNBC.
(a) In vitro induction assay of MDSCs from bone marrow in the presence or absence of IL-34. Bar graphs representing the frequency of M-MDSC ($CD11b^+Ly6C^+Ly6G^-$ cells) and PMN-MDSC ($CD11b^+Ly6C^{lo}Ly6G^+$ cells) within $CD45^+$ cells differentiated from bone marrow (n=3). (b) Subcutaneous tumor growth in BALB/c mice inoculated with Ctrl and IL-34 KO 4T1 cells (1×10^5 cells, n=4-8). Methylpiperidino pyrazole (MPP) (1.0 mg/kg) or control DMSO was administered intraperitoneally daily for 5-14 days. (c) Representative plots of M-MDSC ($CD11b^+Ly6C^+Ly6G^-$ cells) and PMN-MDSC ($CD11b^+Ly6C^{lo}Ly6G^+$ cells) (top). Bar graphs representing the frequency of M-MDSC and PMN-MDSC within $CD45^+$ cells infiltrated in the tumors described in Fig. 2b (n=4-8, bottom). Values were analyzed by a two-sided Student's *t*-test (a) and one-way ANOVA with Tukey's test (b-c) and are shown as mean ± SEM. Asterisk indicates a significant difference; *p<0.05, ***p<0.001, compared with the control group.

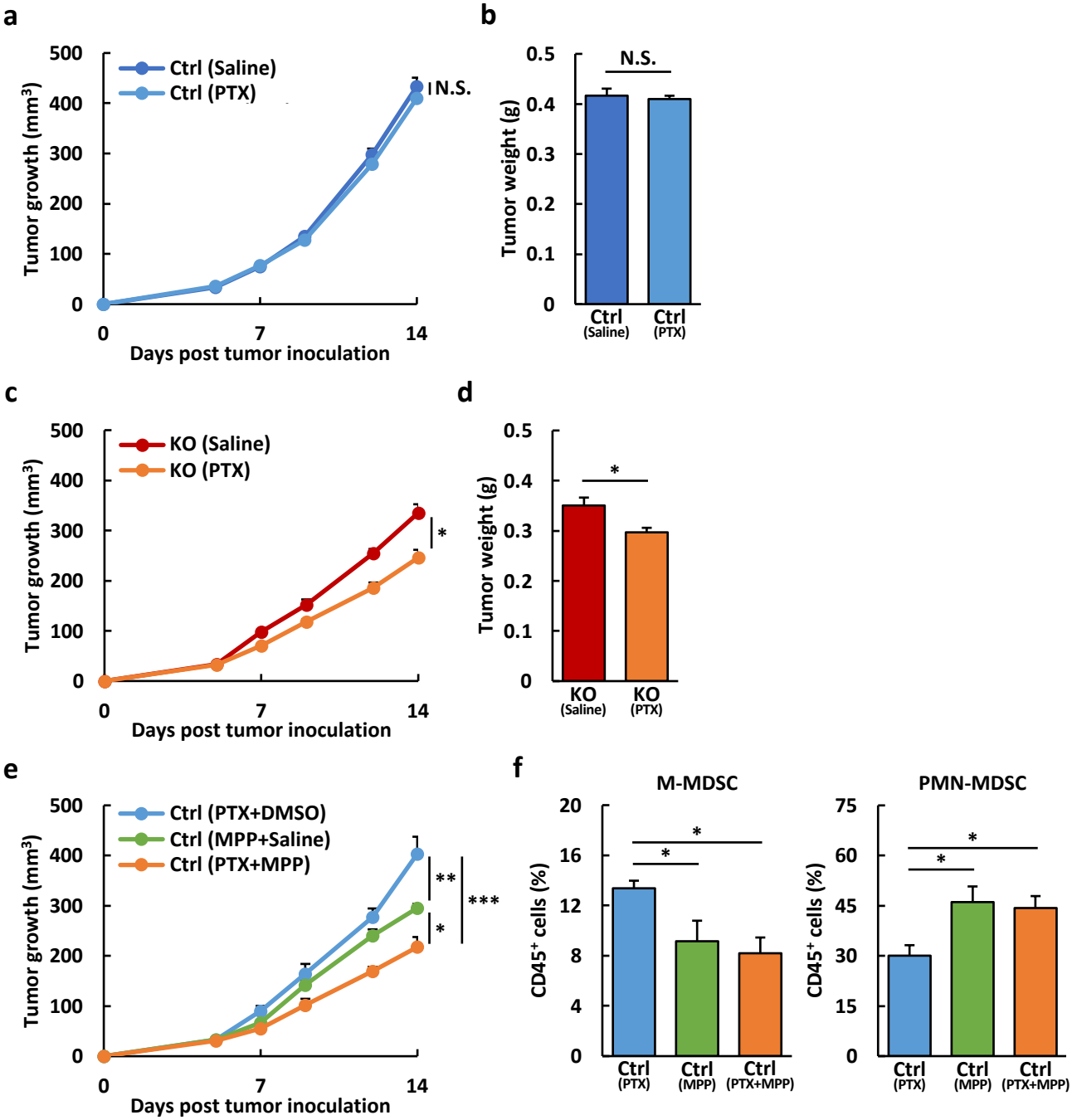

Fig. 3 IL-34-MDSCs axis negates the antitumor effects of Paclitaxel (PTX) in TNBC.

(a) Subcutaneous tumor growth in BALB/c mice inoculated with Ctrl 4T1 cells (1×10^5 cells, n=6). PTX (1.3 mg/kg) or control saline was administered intraperitoneally daily for 5-14 days. (b) Bar graphs representing tumor weight of harvested Ctrl 4T1 tumors at 14 days post tumor inoculation (n=6). (c) Subcutaneous tumor growth in BALB/c mice inoculated with IL-34 KO 4T1 cells (1×10^5 cells, n=6). PTX (1.3 mg/kg) or control Saline was administered intraperitoneally daily for 5-14 days. (d) Bar graphs representing tumor weight of harvested IL-34 KO 4T1 tumors at 14 days post tumor inoculation (n=6). (e) Subcutaneous tumor growth in BALB/c mice inoculated with Ctrl 4T1 cells (1×10^5 cells, n=12). PTX (1.3 mg/kg), control Saline, MPP (1.0 mg/kg), control DMSO, or their combination was administered intraperitoneally daily for 5-14 days. (f) Bar graphs representing the frequency of M-MDSC ($CD11b^+Ly6C^+Ly6G^-$ cells) and PMN-MDSC ($CD11b^+Ly6C^{lo}Ly6G^+$ cells) within $CD45^+$ cells infiltrated in the tumors described in Fig. 3e (n=12). Values were analyzed by a two-sided Student's *t*-test (a-d) and one-way ANOVA with Tukey's test (e-f) and are shown as mean ± SEM. Asterisk indicates a significant difference; *p<0.05, **p<0.01, ***p<0.001, compared with the control group.

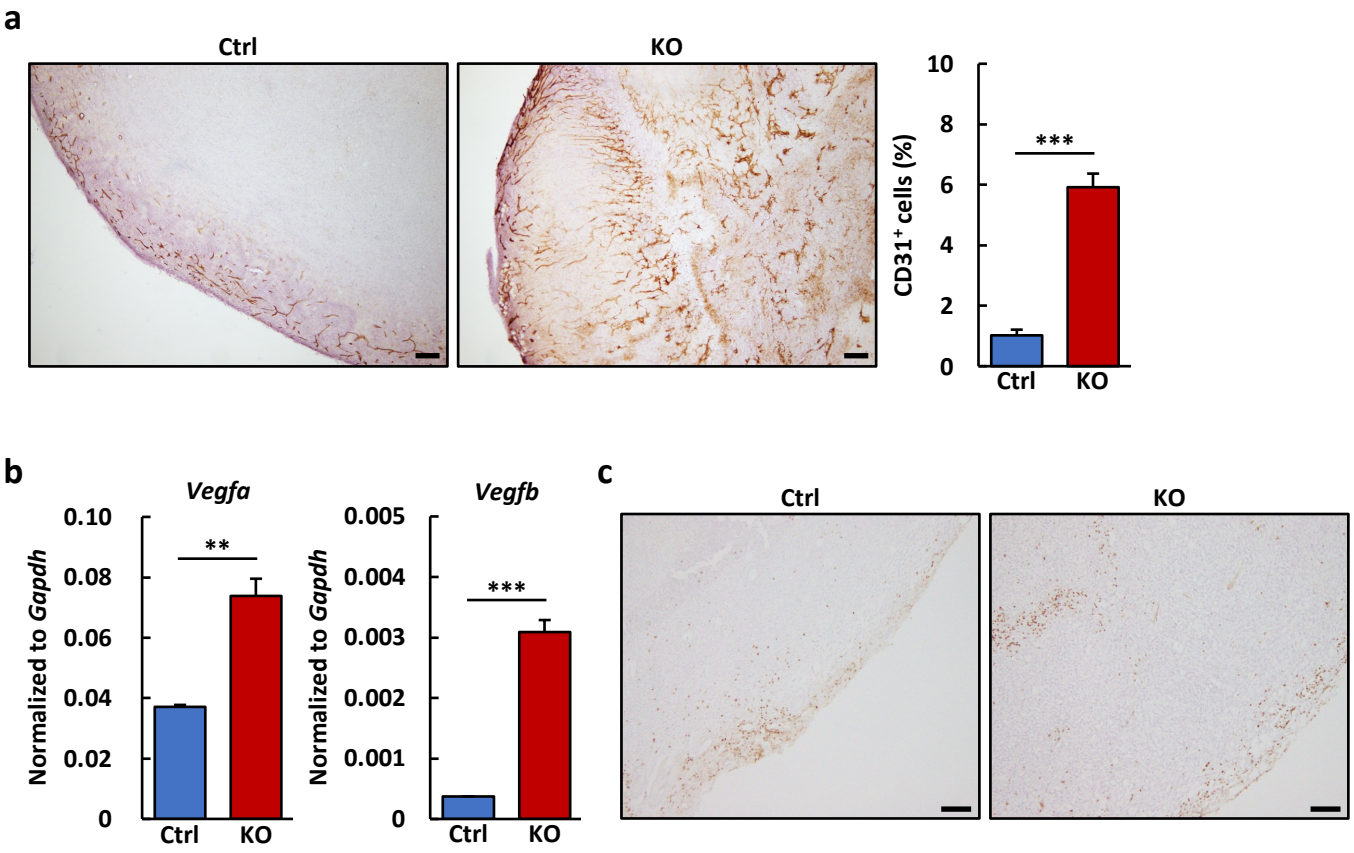

Fig. 4 IL-34-MDSCs axis has the potential to suppress angiogenesis.
(a) Ctrl and IL-34 KO 4T1 cells (1×10^5 cells) were subcutaneously inoculated into BALB/c mice. Representative IHC staining of CD31 (brown) in Ctrl and IL-34 KO 4T1 tumors at the time of day 14 from tumor inoculation (left). Scale bars=200 μm. Quantification of $CD31^+$ cells in Ctrl and IL-34 KO 4T1 tumors from a field of view (n=3, right). (b) PMN-MDSCs were sorted from cell suspensions of tumor-infiltrated immune cells at the time of day 14 from tumor inoculation. Bar graphs representing fold induction of *Vegfa* and *Vegfb* expression of PMN-MDSCs in Ctrl and IL-34 KO 4T1 tumors (n=3). Gene expression levels were determined by RT-PCR, as normalized to *Gapdh*. (c) Representative IHC staining of Gr-1 (brown) in Ctrl and IL-34 KO 4T1 tumors at the time of day 14 from tumor inoculation. Scale bars=100 μm. Values were analyzed by a two-sided Student's *t*-test (a-b) and are shown as mean ± SEM. Asterisk indicates a significant difference; **p<0.01, ***p<0.001, compared with the control group.

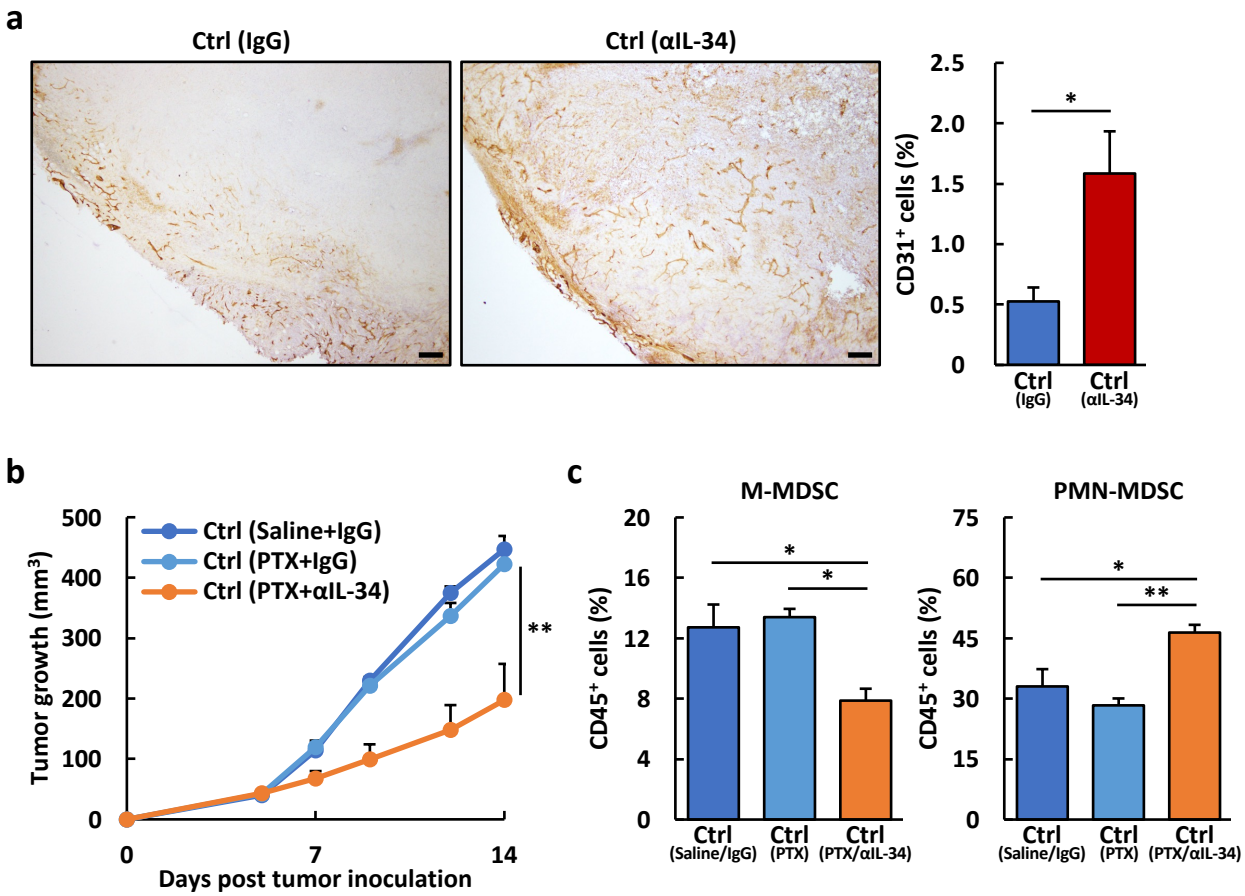

Fig. 5 Effects of IL-34 blockade on chemoresistance including in vivo tumor growth and TME.
(a) Ctrl 4T1 cells (1×10^5 cells) were subcutaneously inoculated into BALB/c mice. Anti-IL-34 antibody (200 μg) or control IgG was administered intraperitoneally daily for 5-14 days. Representative IHC staining of CD31 (brown) in Ctrl 4T1 tumors treated with/without αIL-34 at the time of day 14 from tumor inoculation (left). Scale bars=200 μm. Quantification of $CD31^+$ cells in Ctrl 4T1 tumors treated with/without αIL-34 from a field of view (n=3, right). (b) Subcutaneous tumor growth in BALB/c mice inoculated with Ctrl 4T1 cells (1×10^5 cells, n=12). PTX (1.3 mg/kg), anti-IL-34 antibody (200 μg), control saline, control IgG, or their combination was administered intraperitoneally daily for 5-14 days. (c) Bar graphs representing the frequency of M-MDSC ($CD11b^+Ly6C^+Ly6G^-$ cells) and PMN-MDSC ($CD11b^+Ly6C^{lo}Ly6G^+$ cells) within $CD45^+$ cells infiltrated in the tumors described in Fig. 5b (n=12). Values were analyzed by a two-sided Student's *t*-test (a) and one-way ANOVA with Tukey's test (b-c) and are shown as mean ± SEM. Asterisk indicates a significant difference; *p<0.05, **p<0.01, compared with the control group.

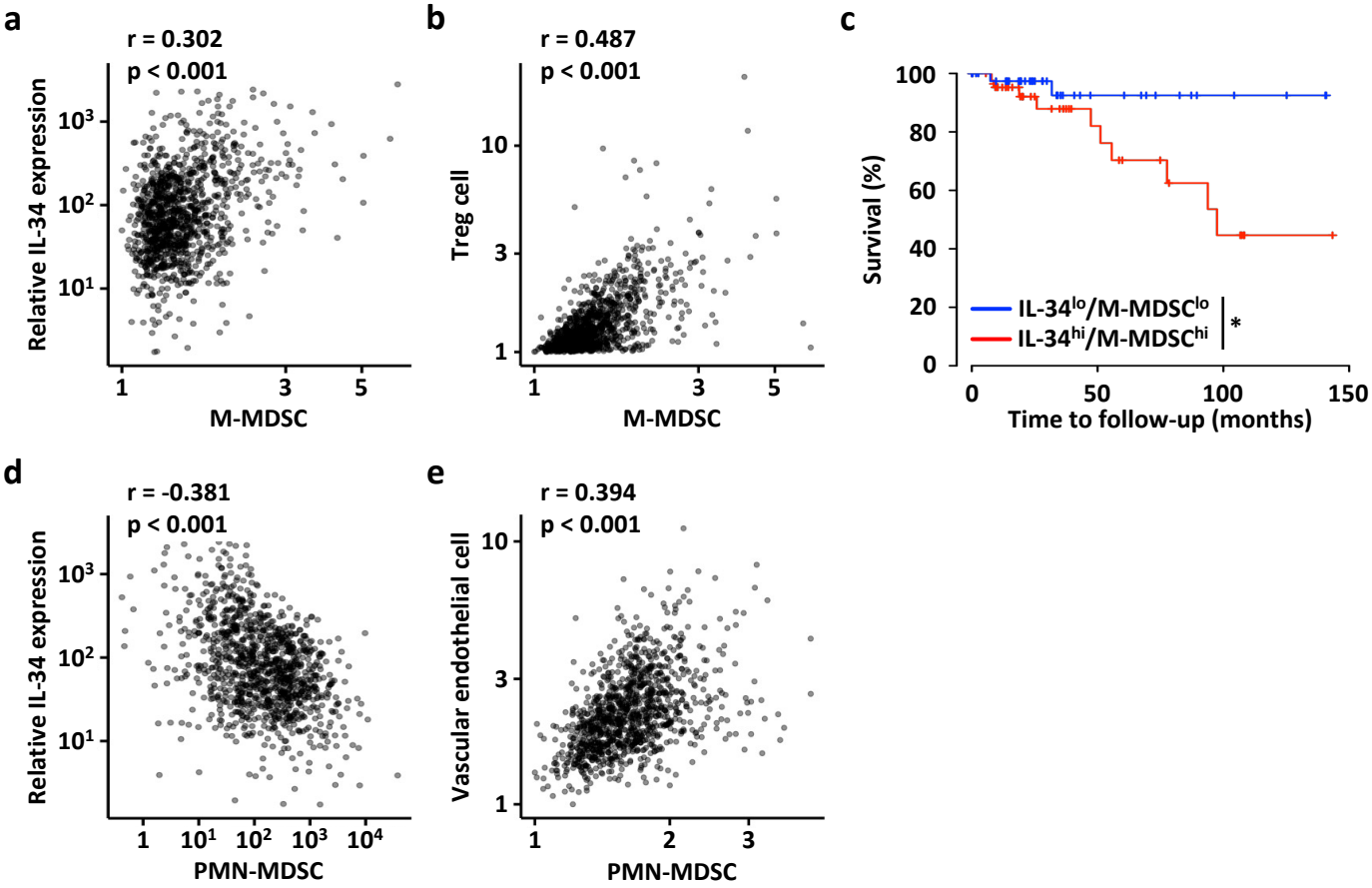

Fig. 6 Potential involvement of IL-34-MDSCs axis in human TNBC.
(a) Pearson correlation coefficient between relative IL-34 expression in tumors and intra-tumoral M-MDSCs infiltration is shown. (b) Pearson correlation coefficient between intra-tumoral Treg cells infiltration and intra-tumoral M-MDSCs infiltration is shown. (c) Kaplan-Meier plot of overall survival of TNBC patients with high IL-34 expression/high M-MDSCs infiltration and low IL-34 expression/low M-MDSCs infiltration stratified by PAM50 subtype. Values were analyzed by a Log-rank test. (d) Spearman correlation coefficient between relative IL-34 expression in tumors and intra-tumoral PMN-MDSCs infiltration is shown. (e) Pearson correlation coefficient between intra-tumoral vascular endothelial cells infiltration and intra-tumoral PMN-MDSCs infiltration is shown.

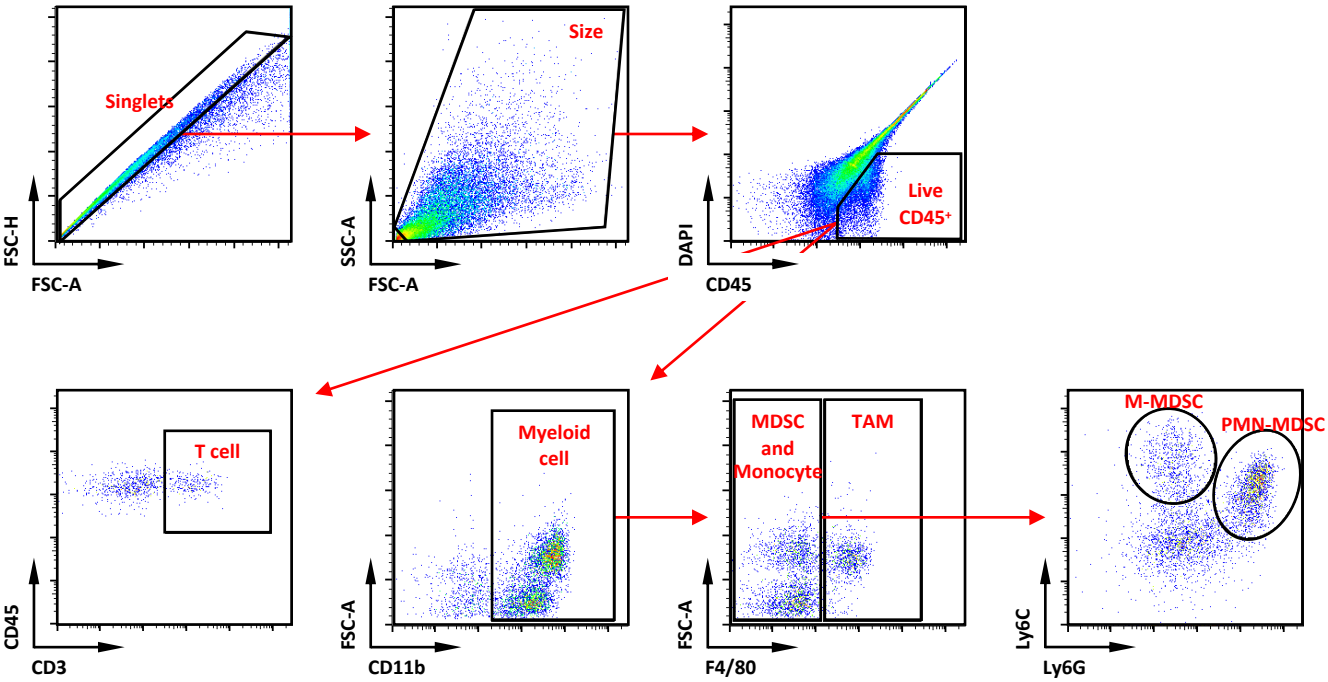

Fig. S1 Flow cytometry gating strategy that used to define each immune cell in the 4T1 tumors.
Singlets were selected from the FSC-A versus FSC-H dot plot, remained-erythrocytes and debris were removed based on FSC-A versus SSC-A, and dead cells were excluded with 4', 6-diamidino-2-phenylindole (DAPI), simultaneously, immune cells were gated on CD45+ cells, then a target population was expanded. The flow cytometry gating strategy used to define T cell ($CD3^+$ cells), TAM ($CD11b^+F4/80^+$ cells), M-MDSC ($CD11b^+F4/80^-Ly6C^+Ly6G^-$ cells), and PMN-MDSC ($CD11b^+F4/80^-Ly6C^{lo}Ly6G^+$ cells) within $CD45^+$ cells infiltrated in the 4T1 tumors.

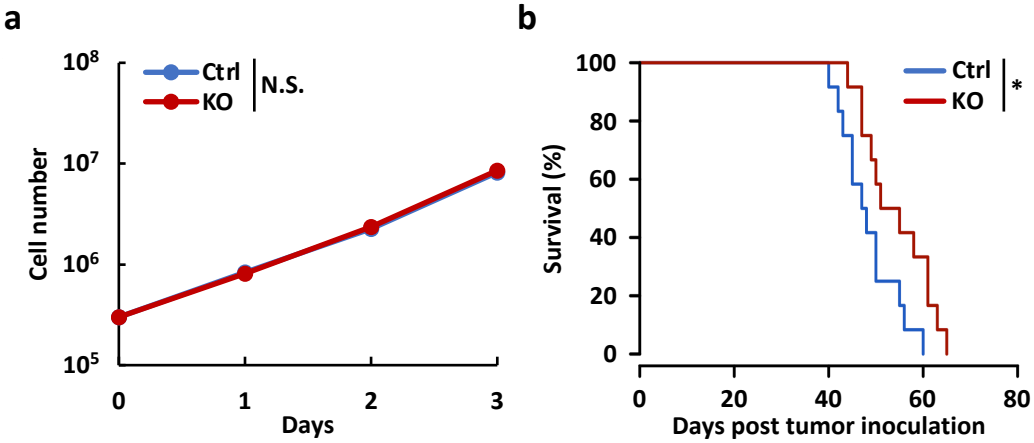

Fig. S2 Effects of IL-34 on in vitro cell proliferation and in vivo survival.
(a) Numbers of Ctrl and IL-34 KO 4T1 cells in cell culture were monitored for 3 days (n=3). (b) Kaplan–Meier plots of survival in mice inoculated with Ctrl and IL-34 KO 4T1 cells (1 x 10^5 cells, n=12). Values were analyzed by a two-sided Student's *t*-test (a) and Log-rank test (b) and are shown as mean ± SEM. Asterisk indicates a significant difference; *p<0.05, compared with the control group.

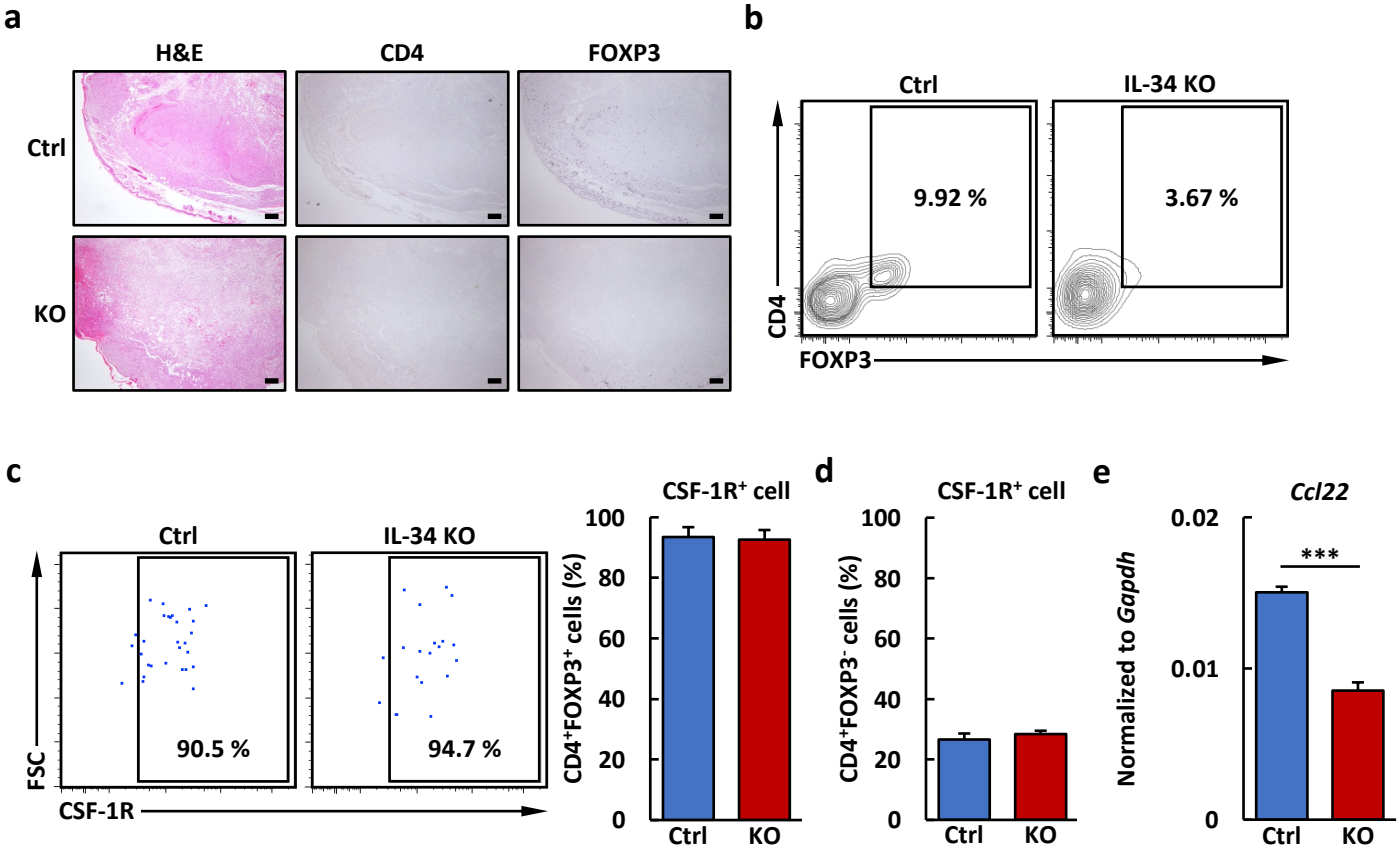

Fig. S3 Potential involvement of IL-34 in intra-tumoral Treg cells induction.

(a) Ctrl and IL-34 KO 4T1 cells (1×10^5 cells) were subcutaneously inoculated into BALB/c mice. Representative staining of H&E, CD4, and FOXP3 in injected Ctrl and IL-34 KO 4T1 tumors at the time of day 14. Scale bars=200 μm. (b) Representative plots of Treg cell ($CD4^+FOXP3^+$ cells) within $CD3^+$ cells infiltrated in the tumors described in Fig. S1a. (c) Representative plots (left). Bar graphs representing the frequency of CSF-$1R^+$ Treg cell ($CD4^+FOXP3^+CSF\text{-}1R^+$ cells) within $CD4^+FOXP3^+$ infiltrated in the tumors described in Fig. S1a (n=3, right). (d) Bar graphs representing the frequency of CSF-$1R^+$ T cell except for Treg cell ($CD4^+FOXP3^-CSF\text{-}1R^+$ cells) within $CD4^+FOXP3^-$ infiltrated in the tumors described in Fig. S1a (n=3). (e) M-MDSCs were sorted from cell suspensions of tumor-infiltrated immune cells at the time of day 14 from tumor inoculation. Bar graphs representing fold induction of *Ccl22* expression of M-MDSCs in Ctrl and IL-34 KO 4T1 tumors (n=3). Gene expression levels were determined by RT-PCR, as normalized to *Gapdh*. Values were analyzed by a two-sided Student's *t*-test (c-e) and are shown as mean ± SEM. Asterisk indicates a significant difference; ***p<0.001, compared with the control group.

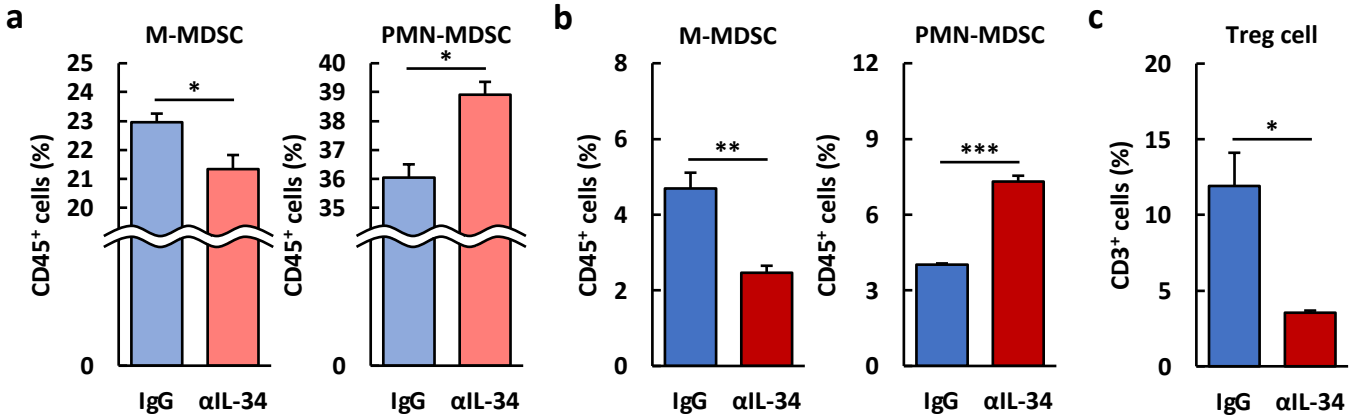

Fig. S4 Effects of IL-34 on TME within breast cancer patient-derived organoids and murine spontaneous TNBC tumors. (a) Anti-IL-34 antibodies (αIL-34) or control IgG were added to breast cancer patient-derived organoids containing immune cells, and MDSCs phenotype within the organoids was observed. Bar graphs representing the frequency of M-MDSC ($CD11b^+CD33^+CD14^+CD15^-$ cells) and PMN-MDSC ($CD11b^+CD33^+CD15^+CD14^-$ cells) within $CD45^+$ cells (n=3). (b) Bar graphs representing the frequency of M-MDSC ($CD11b^+Ly6C^+Ly6G^-$ cells) and PMN-MDSC ($CD11b^+Ly6C^{lo}Ly6G^+$ cells) within $CD45^+$ cells infiltrated in the spontaneous tumors of MMTV-PyMT mice (n=3). (c) Bar graphs representing the frequency of Treg cell ($CD3^+CD4^+FOXP3^+$ cells) within $CD45^+$ cells infiltrated in the spontaneous tumors of MMTV-PyMT mice (n=3). Values were analyzed by a two-sided Student's *t*-test and are shown as mean ± SEM. Asterisk indicates a significant difference; *p<0.05, **p<0.01, ***p<0.001, compared with the control group.

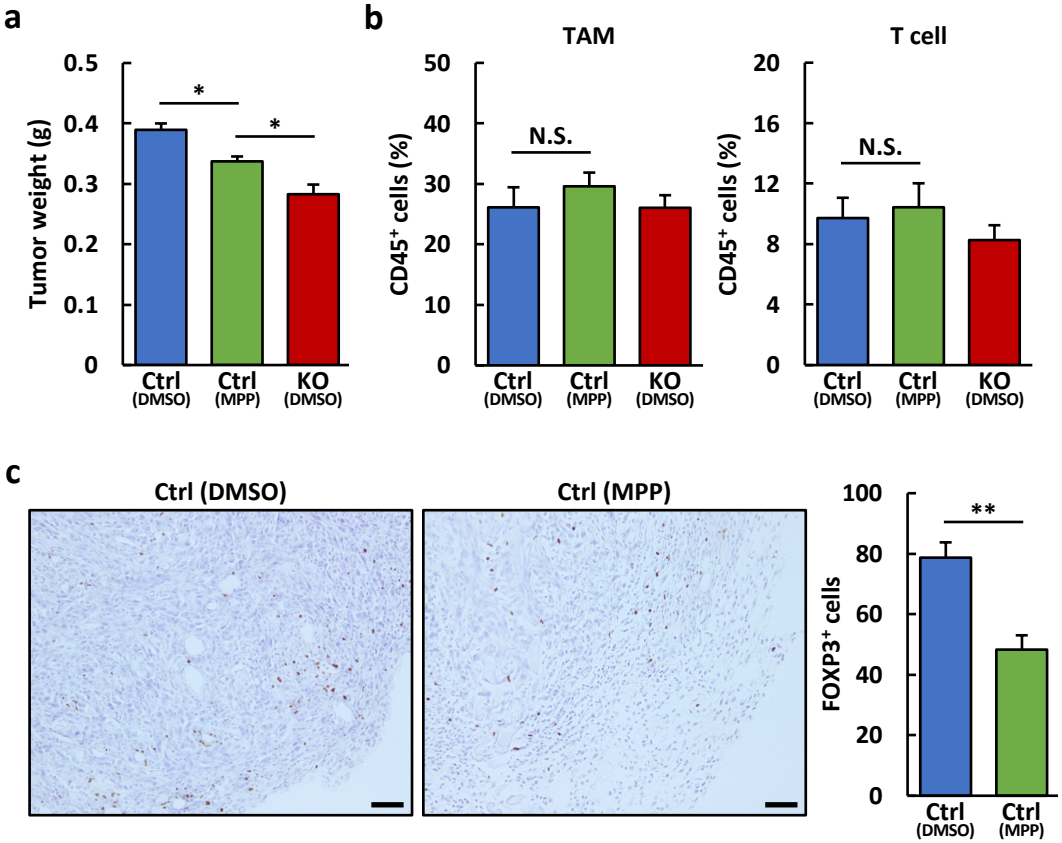

Fig. S5 Effects of MPP administration aimed at M-MDSCs depletion on tumor weight, tumor-infiltrating macrophages, and T cells, including Treg cells.

(a) Ctrl and IL-34 KO 4T1 cells (1×10^5 cells) were subcutaneously inoculated into BALB/c mice. MPP (1.0 mg/kg) or control DMSO was administered intraperitoneally daily for 5-14 days. Bar graphs representing tumor weight of harvested Ctrl and IL-34 KO 4T1 tumors at 14 days post tumor inoculation (n=4-8). (b) Bar graphs representing the frequency of TAM ($CD11b^+F4/80^+$ cells) and T cell ($CD3^+$ cells) within $CD45^+$ cells infiltrated in the tumors described in Fig. S4a (n=4-8). (c) Representative IHC staining of FOXP3 (red) in Ctrl tumors treated with/without MPP at the time of day 14 from tumor inoculation (left). Scale bars=50 μm. Quantification of $FOXP3^+$ cells in Ctrl tumors treated with/without MPP from a field of view (n=3, right). Values were analyzed by a one-way ANOVA with Tukey's test (a-b) and two-sided Student's *t*-test (c) and are shown as mean ± SEM. Asterisk indicates a significant difference; *p<0.05, **p<0.01, compared with the control group.

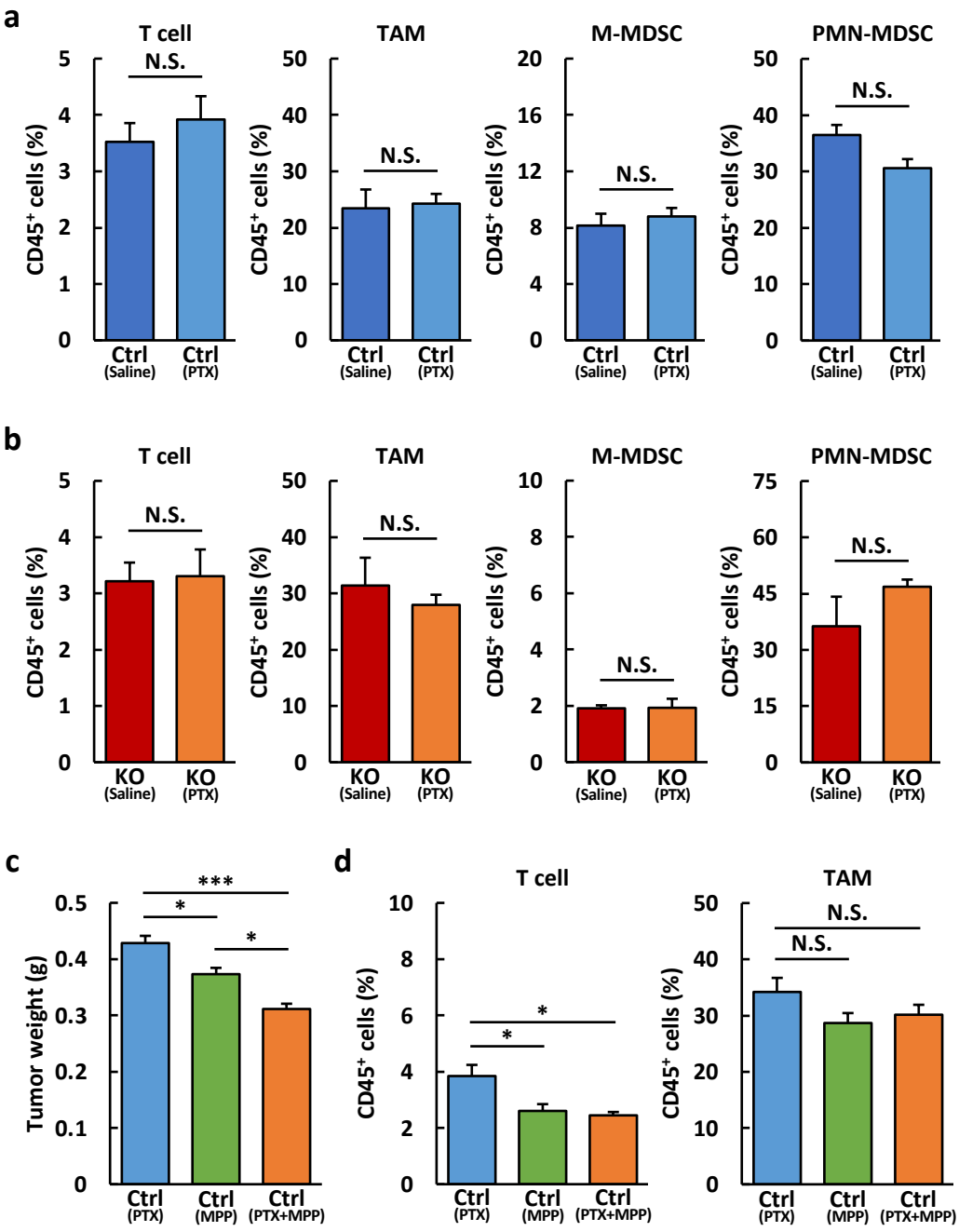

Fig. S6 Effects of PTX and/or MPP treatment on tumor-infiltrating immune cells and tumor weight in Ctrl and IL-34 KO 4T1 tumors.

(a-b) Ctrl and IL-34 KO 4T1 cells (1×10^5 cells) were subcutaneously inoculated into BALB/c mice. PTX (1.3 mg/kg) or control saline was administered intraperitoneally daily for 5-14 days. Bar graphs representing the frequency of T cell ($CD3^+$ cells) and TAM ($CD11b^+F4/80^+$ cells) and M-MDSC ($CD11b^+Ly6C^+Ly6G^-$ cells) and PMN-MDSC ($CD11b^+Ly6C^{lo}Ly6G^+$ cells) within $CD45^+$ cells infiltrated in the Ctrl and IL-34 KO 4T1 tumors (n=6). (c) Ctrl 4T1 cells (1×10^5 cells) were subcutaneously inoculated into BALB/c mice. PTX (1.3 mg/kg), control Saline, MPP (1.0 mg/kg), control DMSO, or their combination was administered intraperitoneally daily for 5-14 days. Bar graphs representing tumor weight of harvested Ctrl 4T1 tumors at 14 days post tumor inoculation (n=12). (d) Bar graphs representing the frequency of T cell ($CD3^+$ cells) and TAM ($CD11b^+F4/80^+$ cells) within $CD45^+$ cells infiltrated in the Ctrl 4T1 tumors (n=12). Values were analyzed by a two-sided Student's *t*-test (a-b) and one-way ANOVA with Tukey's test (c-d) and are shown as mean ± SEM. Asterisk indicates a significant difference; *p<0.05, ***p<0.001, compared with the control group.

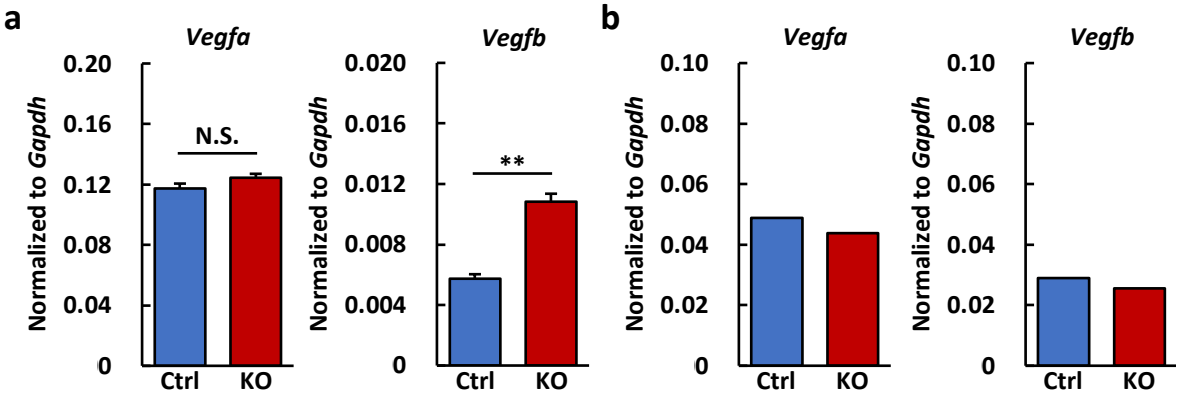

Fig. S7 The angiogenic ability of M-MDSCs and cancer cells in the presence or absence of IL-34.
(a) M-MDSCs were sorted from cell suspensions of tumor-infiltrated immune cells at the time of day 14 from tumor inoculation. Bar graphs representing fold induction of *Vegfa* and *Vegfb* expression of M-MDSCs in Ctrl and IL-34 KO 4T1 tumors (n=3). Gene expression levels were determined by RT-PCR, as normalized to *Gapdh*. (b) Bar graphs representing fold induction of *Vegfa* and *Vegfb* expression of Ctrl and IL-34 KO 4T1 cells. Gene expression levels were determined by RT-PCR, as normalized to *Gapdh*. Values were analyzed by a two-sided Student's *t*-test (a-b) and are shown as mean ± SEM. Asterisk indicates a significant difference; **p<0.01, compared with the control group.

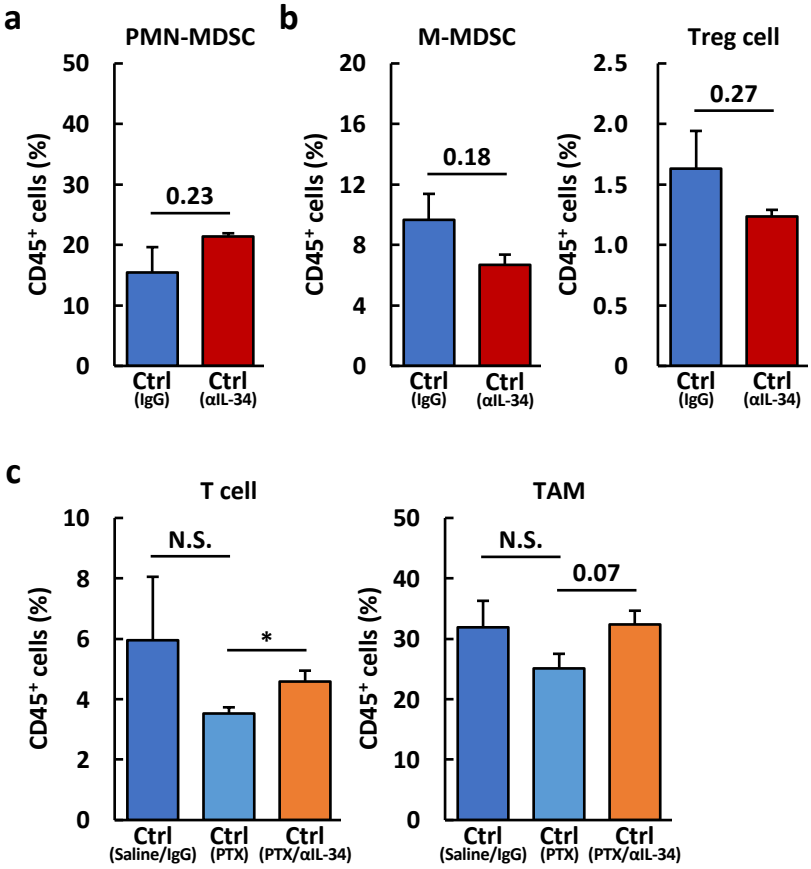

Fig. S8 Effects of IL-34 blockade and/or PTX treatment on tumor-infiltrating immune cells in Ctrl 4T1 tumors.
(a-b) Ctrl 4T1 cells (1×10^5 cells) were subcutaneously inoculated into BALB/c mice. Anti-IL-34 antibody (200 μg) or control IgG was administered intraperitoneally daily for 5-14 days. Bar graphs representing the frequency of PMN-MDSC ($CD11b^+Ly6C^{lo}Ly6G^+$ cells) and M-MDSC ($CD11b^+Ly6C^+Ly6G^-$ cells) and Treg cell ($CD3^+CD4^+FOXP3^+$ cells) within $CD45^+$ cells infiltrated in Ctrl 4T1 tumors treated with/without αIL-34 (n=6). (c) Bar graphs representing the frequency of T cell ($CD3^+$ cells) and TAM ($CD11b^+F4/80^+$ cells) within $CD45^+$ cells infiltrated in the tumors described in Fig. 5b (n=6-12). Values were analyzed by a two-sided Student's *t*-test (a-b) and one-way ANOVA with Tukey's test (c) and are shown as mean ± SEM. Asterisk indicates a significant difference; *p<0.05, compared with the control group.

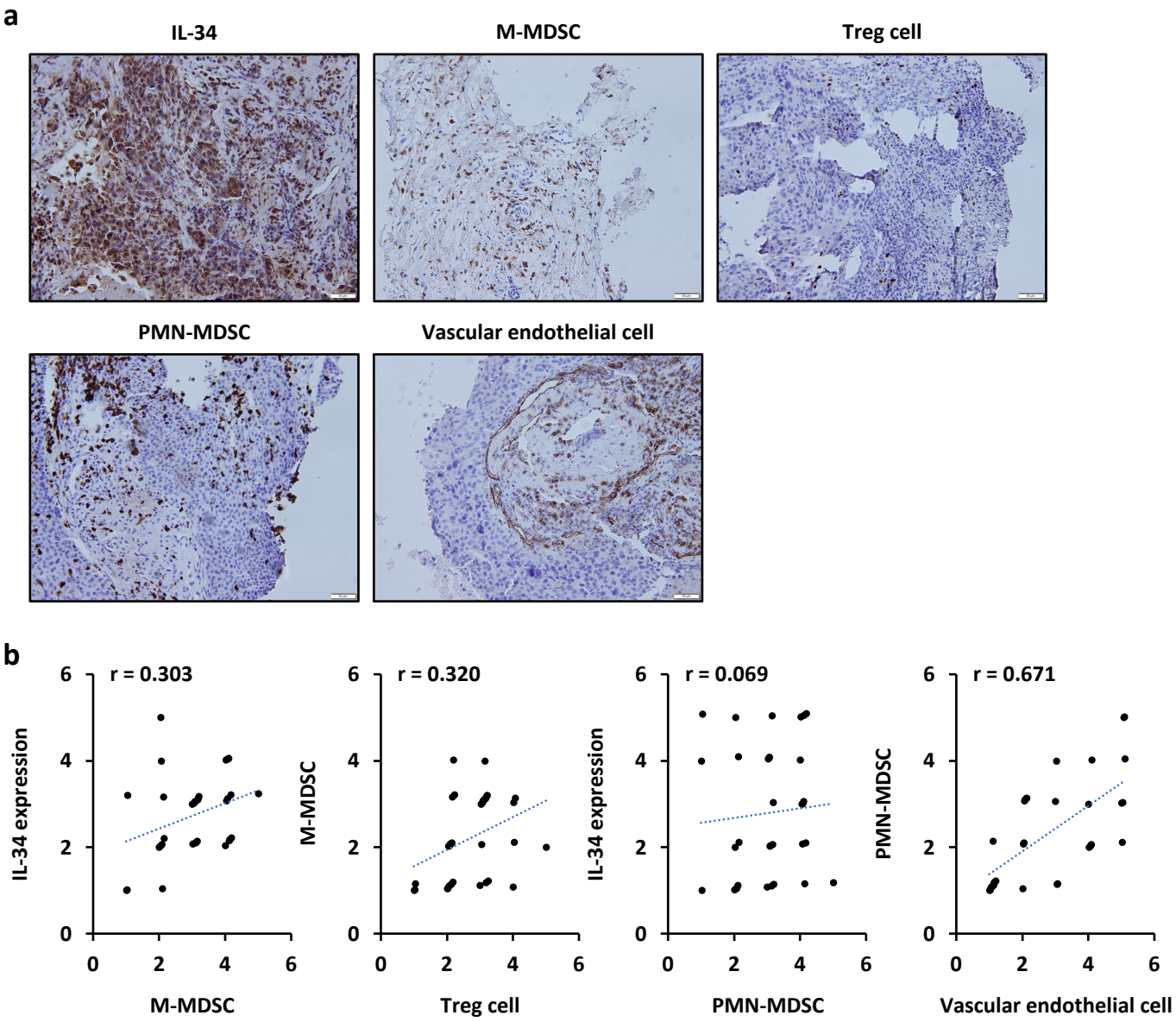

Fig. S9 Potential involvement of IL-34-MDSCs axis in real-world human TNBC.
(a) Representative staining of IL-34, CD14 (used as M-MDSC marker), FOXP3 (used as Treg cell marker), CD15 (used as PMN-MDSC marker), and CD31 (used as vascular endothelial cell marker) in formalin-fixed paraffin-embedded TNBC tissues. Scale bars=50 μm. (b) Pearson correlation coefficient between IL-34 expression in tumors and intra-tumoral M-MDSCs infiltration, intra-tumoral M-MDSCs infiltration and intra-tumoral Treg cells infiltration, IL-34 expression in tumors and intra-tumoral PMN-MDSCs infiltration, intra-tumoral PMN-MDSCs infiltration and intra-tumoral vascular endothelial cells infiltration are shown.